Order Number 9512520

Effect of disorder on the vortex dynamics in superconducting Josephson junction arrays and clusters

Rao, Subashri Vijendran, Ph.D.

University of Illinois at Urbana-Champaign, 1994

U·M·I
300 N. Zeeb Rd.
Ann Arbor, MI 48106

EFFECT OF DISORDER ON THE VORTEX DYNAMICS IN SUPERCONDUCTING JOSEPHSON JUNCTION ARRAYS AND CLUSTERS

BY

SUBASHRI VIJENDRAN RAO

B. Tech., Indian Institute of Technology, Bombay, 1987
M. S., University of Illinois at Urbana-Champaign, 1988

THESIS

Submitted in partial fulfillment of the requirements
for the degree of the Doctor of Philosophy in Physics
in the Graduate College of the
University of Illinois at Urbana-Champaign, 1994

Urbana, Illinois

UNIVERSITY OF ILLINOIS AT URBANA-CHAMPAIGN

THE GRADUATE COLLEGE

MAY 1994

WE HEREBY RECOMMEND THAT THE THESIS BY

SUBASHRI VIJENDRAN RAO

ENTITLED EFFECT OF DISORDER ON THE VORTEX DYNAMICS OF JOSEPHSON JUNCTION ARRAYS AND CLUSTERS

BE ACCEPTED IN PARTIAL FULFILLMENT OF THE REQUIREMENTS FOR THE DEGREE OF DOCTOR OF PHILOSOPHY

Director of Thesis Research

Head of Department

Committee on Final Examination†

Chairperson

† Required for doctor's degree but not for master's.

O-517

EFFECT OF DISORDER ON THE VORTEX DYNAMICS IN SUPERCONDUCTING JOSEPHSON JUNCTION ARRAYS AND CLUSTERS

Subashri Vijendran Rao, Ph. D
Department of Physics
University of Illinois at Urbana-Champaign, 1987
Dale J. Van Harlingen, Advisor

We have studied the effect of intrinsic disorder on the transport properties of large Josephson junction arrays and clusters. In large arrays, intrinsic random disorder results in the washing out of features in the magnetoresistance. It also gives rise to multiple onsets in the resistive transition as a function of temperature. Large arrays are difficult to model because of the large number of junctions involved, thus we have studied the effect of local (single junction) disorder in smaller arrays referred to as clusters. The transport measurements on clusters indicate that features due to disorder in the junction critical currents, dominate the properties. We have developed a simple model in real space to understand the static vortex configurations and the motion of the vortices.

ACKNOWLEDGMENTS

I would like to thank my thesis advisor, Dr. Dale J. Van Harlingen for his patience and understanding. I greatly appreciate his gentle yet persuasive research style.

Gratitude and thanks are also due to my parents and sister for their unconditional love and support at every stage of my career.

The presence of good co-workers went a long way in relieving the stress of working in an otherwise impersonal research atmosphere. Thanks to Fred Sharifi for teaching me the ropes, to Lan Vu for his motivational and entertaining spiels, to Stuart Tessmer for supporting me through annoying equipment failure and dismal data runs, to Ralph Schweinfurth for unusual music and conversation during thesis writing, to Joe Walko for interesting discussions on non-Physics topics, to Dave Wollman for his suggestions, and to Mark Wistrom who made my final year bearable!

I would also like thank my friends, Tanuja, Abhay, Sanjay, Kanth, B, Shaku, Karuna, Tarun and many others for the late night walks, talks, long phone conversations, movies, and good food.

This work was supported by the National Science Foundation through Grant No. NSF-DMR-87-22080 and NSF-DMR-91-15411. The Materials Research Laboratory provided the cleanroom and microfabrication facilities without which this work would have been impossible.

TABLE OF CONTENTS

CHAPTER 1

INTRODUCTION

Superconductivity has been known to mankind for over eighty years now (since its discovery by Kamerlingh Onnes in 1911). Some metals (and recently, even oxides and ceramics) show this property below a certain critical temperature which varies from material to material. The onset of the superconducting transition is signalled by the complete expulsion of magnetic field (the Meissner effect) and zero measurable resistance. In Type II superconductors, above a lower critical field, it is energetically favorable for the system to let the magnetic field penetrate the system and form quantized flux tubes, referred to as vortices. The equilibrium and dynamic properties of the superconductor can be interpreted in terms of the vortices. The discovery of high temperature superconductors (HTSC) has resulted in a renewal of interest in the physics of vortex dynamics.

Thin film, granular superconductors (Type II) are of particular interest. Extensive investigation of HTSC show that they have an intrinsic two-dimensional character similar to thin films. These films are highly granular at the microscopic level, consisting of grains of superconductor separated by boundaries of either insulators (oxides) or normal metal. Two such superconducting grains, separated by a barrier, constitute a weak link (Josephson junction). The weak links in a granular film are arranged in random order. Because of this high degree of disorder, it is extremely difficult to characterize the system. This has resulted in a need for experimental systems where the randomness or disorder can be introduced in a controlled manner. Advances in microlithography and fabrication techniques make it possible to tailor-make arrays with grains of superconductors in a regular periodic lattice pattern with a normal metal or insulator in between. The amount of disorder can be externally controlled.

The array properties are largely governed by the interactive coupling of hundreds of junctions in various network-like configurations. The Hamiltonian for this system is similar to the XY model for spin systems. The array exhibits long range order and phase coherence. Chapter 2 is a brief review of the theory of Josephson junction arrays. The individual properties of the junctions and the effect of having Josephson junctions in a superconducting loop are studied. The theories describing the static properties (equilibrium vortex configurations) and the dynamic properties (vortex motion) are discussed in detail.

In Chapter 3, transport measurements on large (500 x 500) square Josephson junction arrays are presented. The data reflects the effects of intrinsic disorder on both the resistive transition and the magnetoresistance. Various theories have been proposed to analyze the resistive transition. The theories use mean field calculations to predict the resistive transition for different temperature regimes because the array system is too complex to perform calculations from first principles. This gap between the measured and the calculated quantities has long been a stumbling block in the study of Josephson junction arrays.

A better understanding of the local properties, effect of finite number of vortices, and the junction phases can be obtained by studying a smaller group of junctions where the data can be directly compared with theoretical models obtained from first principle calculations. Chapter 4 presents an in-depth study of small arrays of Josephson junctions, referred to as clusters. Magnetoresistance measurements for clusters of different sizes exhibit the effect of cluster size and individual junction effects. Computer simulations of both the energy (static) and voltage (dynamical) simulations (as a function of magnetic field and current) have been made based on first principle calculations to compare with the experimental data. The role of bond disorder is discussed.

Josephson junction arrays continue to be of great interest to both experimentalists and theorists because of their rich and complex geometry. A lot of work has already been done to unravel their mysteries and yet major questions remain unanswered. The exact nature of vortex motion and the shape of the array potential in real space are still unknown. An effort should be made to translate the evolution of phases in multi-dimensional phase space (of the junctions) to actual vortex motion in two-dimensional real space. We have made a beginning by looking at clusters (small arrays). These studies are also of great relevance in understanding HTSC films. The future of this field is largely dependent on whether this knowledge can be applied towards creating viable devices that improve on the existing technology.

CHAPTER 2

THEORY

Large Josephson Junction arrays have been studied as model systems for granular superconductors and thin films as discussed in Chapter 1.[1] The properties of the array reflect the effect of both the individual junctions and the effect of collective behavior of many junctions in a network configuration. The Hamiltonian of the array can be controlled externally by a magnetic field. It is also possible to fabricate arrays of different geometries with desired amounts of uniformity (or randomness). This ability to control parameters makes Josephson arrays useful model systems. In the following sections, the Josephson junction equations, flux quantization requirements, phase coherence across the array, and the nature of the resistive transition are discussed.

2.1 Phase and the Josephson Junction

The essential universal characteristic of the superconducting state is the existence of the many particle condensate wave function, $\psi(\vec{r}) = |\psi(\vec{r})|e^{i\phi(\vec{r})}$ which has an amplitude $|\psi(\vec{r})|$ and a macroscopic phase $\phi(\vec{r})$. An isolated superconductor can therefore be defined by a single wavefunction and a macroscopic phase. This condensate is analogous to the familiar Bose-Einstein condensate.

The basic building block of an array is a Josephson junction.[2] Figure 2.1 shows some typical geometries of Josephson junction arrays. Our arrays consist of Superconductor - Normal - Superconductor (S-N-S) junctions. If the normal metal is

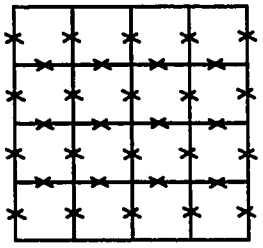

Square

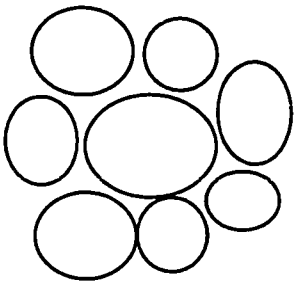

Superconducting grains

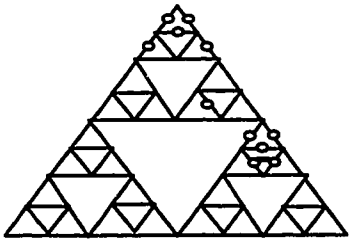

Fractal

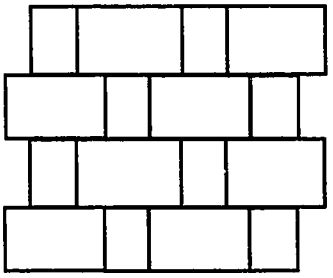

Quasi-periodic

Fig: 2.1 Some typical geometries for Josephson junction arrays

thin enough, the S-N-S junction can support a non-dissipative supercurrent. This is possible because of the proximity effect. The black lines are superconducting ; x and • represent the Josephson junctions.

The proximity effect is observed at the interface of a superconductor and a normal metal, semiconductor or a weaker superconductor (not insulator) as illustrated in Figure 2.2. The presence of the normal metal suppresses the wave function in the superconductor near the interface. The wave function is continuous at the interface but the pair potential can be discontinuous. There is a leakage of Cooper pairs from the superconductor into the normal metal and a leakage of the quasiparticles from the normal metal into the superconductor. The pair condensate wave function in the superconductor leaks into the normal metal and decays exponentially over a characteristic length referred to as the normal metal coherence length ξ_N.

The Josephson effect depends on the existence of a weak connection between the wave functions on either sides of the junction which can happen if the normal metal thickness is of the order of the coherence length. The junction can then support a supercurrent. The coupling energy E_c is given by

$$E_c = -E_J \cos(\phi_i - \phi_j) \tag{2.1}$$

where E_J is the Josephson energy and ϕ_i and ϕ_j are the macroscopic phases of the two superconductors that have been defined previously. The supercurrent through the junction is

$$I_S = I_o \sin(\phi_i - \phi_j) \tag{2.2}$$

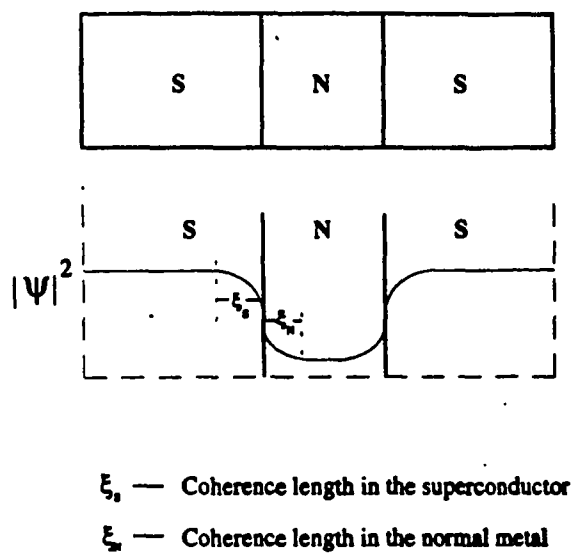

ξ_s — Coherence length in the superconductor

ξ_n — Coherence length in the normal metal

Fig: 2.2 Proximity effect at a superconductor-normal interface

S - Superconductor ; N - Normal metal $|\psi|^2$ is the superconducting pair density

where I_o is the maximum supercurrent, otherwise referred to as the critical current. This is the first Josephson relation. The Josephson coupling energy E_J, is related to the critical current I_o through $E_J = \frac{\hbar}{2e} I_o$. The voltage across the junction is proportional to the time rate of change of the phase difference.

$$V = \frac{\hbar}{2e} \frac{d\phi_{ij}}{dt} \tag{2.3}$$

This is the second Josephson relation where $\phi_{ij} = \phi_i - \phi_j$.

These equations are modified in the presence of a magnetic field. The field contributes a phase factor through the integral of the vector potential across the junction. The phase is then redefined as

$$\phi_{ij} = \phi_i - \phi_j - \psi_{ij} \tag{2.4}$$

where $\psi_{ij} = \frac{4\pi e}{h} \int_j^i \vec{A} \cdot \vec{dl}$, and $\vec{A}$ is the vector potential.

2.2 Resistively Shunted Junction (RSJ) Model.

The RSJ model was proposed by W. C. Stewart[3] and D. E. McCumber[4] to take the finite junction size and the normal current into account. In this model, a Josephson junction can be modelled as composed of three components: a superconducting part that obeys the Josephson relations, a shunt capacitance associated with the junction size, and a shunt resistance associated with the normal current (Fig: 2.3(a)). For a total bias current I_b through the junction, current conservation requires that

$$I_b = I_S + I_R + I_C \tag{2.5}$$

where I_R is the current through the shunt resistance, I_C is the current through the capacitor. For a voltage V across the junction and $i_b = I_b / I_o$

$$i_b - \sin(\phi_{ij}) = \frac{V}{RI_o} + \frac{C}{I_o}\frac{dV}{dt} \tag{2.6}$$

Defining a potential $U(\phi)$ such that $U(\phi_{ij}) = -E_J(i_b\phi_{ij} + \cos(\phi_{ij}))$, and using the second Josephson relation, we can rewrite the current conservation equation as

$$(i_b - \sin(\phi_{ij})) = [-\frac{1}{E_J}\frac{dU(\phi_{ij})}{d\phi_{ij}} = \frac{d\phi_{ij}}{d\tau} + \beta_c\frac{d^2\phi_{ij}}{d\tau^2}\ ] \tag{2.7}$$

This is a second order differential equation which gives the energy $U(\phi_{ij})$ for a "particle" moving in a one dimensional potential in phase (ϕ) space with a mass proportional to the junction capacitance C. The potential $U(\phi_{ij})$ is depicted in Fig: 2.3(b) for different bias currents and is referred to as the washboard potential. Note that as the bias current is increased, the washboard "tips" and at the critical current, the local minima disappear completely. The "mass" is now free to roll down the potential and this results in a non-zero voltage. The normalized time τ is $\frac{\hbar}{2eI_oR}$. The damping coefficient is proportional to 1/R. The parameter β_c is the McCumber-Stewart parameter which is defined as $\beta_c = \frac{2eI_oR^2C}{\hbar}$. For an S-N-S junction, the shunt resistance is small and we can ignore the capacitance.

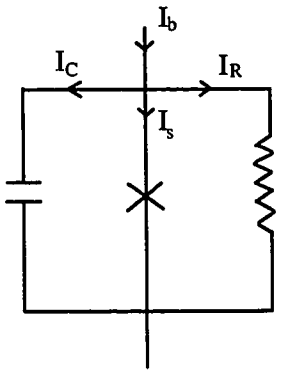

Fig: 2.3 (a) The RSJ model

Fig: 2.3 (b) The Washboard Potential

2.3 Flux Quantization

One of the basic implications of the superconducting wave function $\psi(\vec{r}) \equiv |\psi(\vec{r})| e^{i\phi(\vec{r})}$, is the single valuedness of the macroscopic phase $\phi(\vec{r})$. $\phi(\vec{r})$ has to return to modulo 2π on going around a closed superconducting loop. This requirement leads to a striking demonstration of the quantum-mechanical properties of the superconducting state which is the quantization of magnetic flux in a superconducting loop.

The quantization requirement depends on the nature of the superconducting loop. In the case of a superconducting loop deep inside a bulk superconductor (where the supercurrent is zero), the gauge-invariant phase drop

$$\Delta\phi = [\, -\oint \vec{\nabla}\phi \cdot \vec{dl} - \frac{2e}{\hbar}\int \vec{A}.\vec{dl} \,] = 0$$

The single-valuedness of the wave function then requires that the net phase drop be a multiple of 2π

$$\begin{aligned} 2\pi n &= -\oint \vec{\nabla}\phi.\vec{dl} = \frac{2e}{\hbar}\oint \vec{A}\cdot\vec{dl} \\ \frac{nh}{2e} &= \oint \vec{A}\cdot\vec{dl} \end{aligned} \qquad (2.8)$$

Defining $\Phi_o = h / 2e$, this equation gives the flux quantization requirement. Φ_o(which is $2.07\text{x}10^{-7}\,\text{G}-\text{cm}^2$) is the flux quantum. In other words, the flux through a superconducting ring takes only discrete values. Hence a ring cooled below its transition temperature in a magnetic field will generate circulating currents that add or subtract flux to bring the total to an integral number of flux quanta. The ratio of the external magnetic flux Φ to one flux quantum Φ_o is referred to as the frustration factor f ($f = \Phi/\Phi_o$).

The vortex in a thin film or bulk superconductor consists of a normal core surrounded by a superconducting region with a supercurrent that contributes to the flux. Figure 2.4 (a), gives the spatial extent of the vortex core and the field for an isolated vortex. The spatial extent of the core is defined as the coherence length. The lines of force due to the enclosed magnetic field are not confined to the normal core. The field is a maximum at the center but extends a distance equal to the penetration depth in that material.

This requirement is modified for the case of a superconducting loop with weak links (Figure 2.4 (b)). The net phase drop around the loop now has additional terms from the discrete phase drop across the weak links and contribution of the supercurrent to the field through the loop inductance. The weak link contribution is the previously defined ϕ_{ij} (equation 2.3). The net phase drop around the loop is given by flux quantization requirement.

$$\oint \vec{\nabla}\phi.\vec{dl} = \sum_{ij}\phi_{ij} - \frac{2e}{\hbar}\oint \vec{A}\cdot\vec{dl} - \frac{2\pi LJ_S}{\Phi_O} = 2\pi n \qquad (2.9)$$

where L is the inductance and $\phi_{ij} = \phi_i - \phi_j - \frac{2e}{\hbar}\int \vec{A}\cdot\vec{dl}$. The sum of the phase drops is only over nearest neighbors. The quantity that is now quantized is not just a flux term but what is referred to as the fluxoid. The vortex is a combination of discrete phase drops and induced fields. The "core" of the vortex is now just the loop area. The coherence length, in this case is of the order of the cell size. For the weakly coupled superconducting array, the inductance contribution is small and can be neglected. The phase drop across the individual junctions gives the main contribution to the "fluxoid".

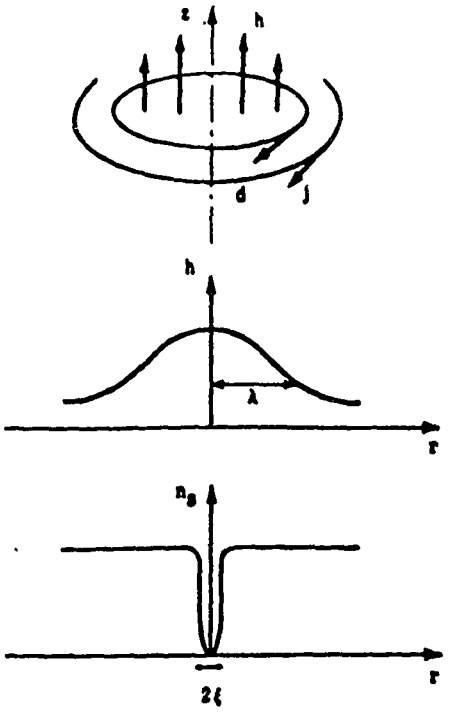

Fig: 2.4 (a) The spatial distribution of the vortex in a Type II superconductor

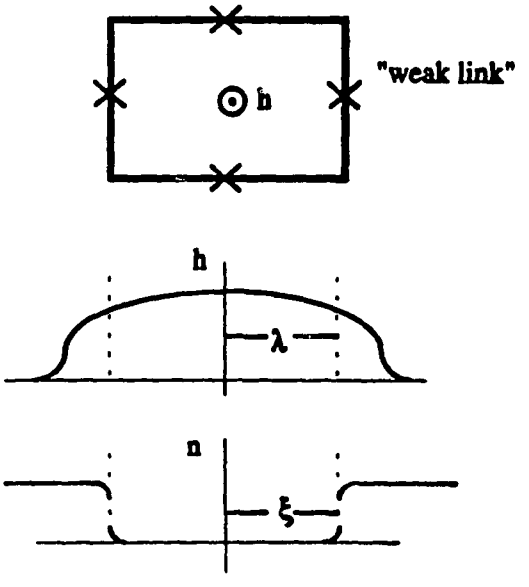

Fig: 2.4 (b) The "vortex" enclosed in a thin superconducting ring with weak links

An array of Josephson junctions consists of many such superconducting loops in a regular pattern. A single loop is the basic array unit and is referred to as a cell. The depth in the transverse direction $\lambda_\perp$ which is given by $\lambda_\perp = \frac{\lambda^2}{2d}$. The bulk penetration λ, is the distance to which the magnetic field penetrates into the superconductor before it effects of the vortices in both cases is however the same. The relevant penetration depth in these two-dimensional systems is the magnetic penetration drops to 1/e of its original value and d is the thickness of the film. For a weakly coupled array, the transverse penetration depth is of the order of the sample size. Hence vortex-vortex interactions play an important role in determining the array properties.

2.4 Vortex Pinning in Josephson Junction Arrays

The Josephson junction array provides a uniform lattice of vortex pinning sites. It is energetically favorable for the vortex to be in a cell rather than on a junction. The junction acts as a barrier to vortex motion and the barrier height is defined as the difference in the energies of a vortex on a junction and the vortex in the cell. For the case of a vortex crossing an isolated junction, the barrier height is E_J. The barrier height is quite different for the case of the Josephson junction array which consists of hundreds of junctions.

Lobb et al[2] calculated the barrier height E_B for an infinite square array to be 0.2 E_J. In this model, the total energy (Hamiltonian) of the system is the sum of the individual junction energies

$$H = E_J \sum_{ij} [\, 1 - \cos (\phi_i - \phi_j - \frac{2e}{\hbar} \int \vec{A} \cdot \vec{dl})] \qquad (2.10)$$

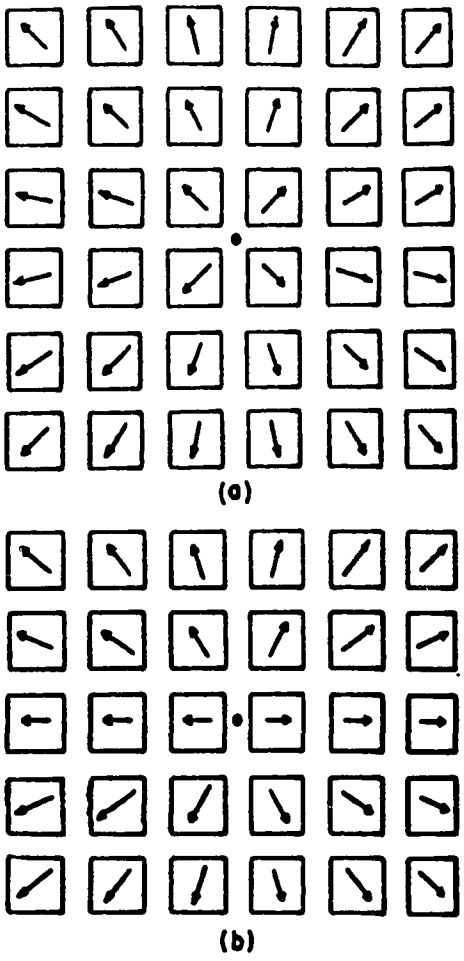

Superconducting Island • vortex

→ Phase of the island corresponds to the angle made with the x axis

Fig: 2.5: Phase Configurations for vortex centers located

a) at the center of four superconducting islands b) in the space between adjacent islands .

To obtain the barrier height, the phases ϕ_i across the junctions due to the vortices need to be defined. Figures 2.5 (a) and (b) show the two phase configurations corresponding to vortex centers located in the center of the cell and on the junction respectively. In both configurations, the phase at very large r is known by symmetry to be $\phi(r) = \tan^{-1}(y / x)$. For the configuration in Figure 2.5 (a), symmetry requires that the phase vectors on the four islands nearest the center, point radially outward. For the configuration in Figure 2.5 (b), the phase angle is 0 for islands on the line to the right and π for those to the left. To find the phase at all the other islands, using the "arctan" approximation to the vortex phase configuration, Rzchowski et al[3] made a sinusoidal approximation for the vortex potential. For a vortex located at (x_o, y_o), the phase is given by

$$\phi_i = \arctan\ [(y_i - y_o) / (x_i - x_o)], \tag{2.11}$$

and this is used to obtain the energy of the system for various vortex center configurations. The spatial potential distribution can be calculated by looking at the contribution of one junction to the system energy for various vortex positions around the junction is considered. The problem can be recast as a particle moving in a square array of repulsive "molecules" that are centered on each junction. This gives the spatial potential distribution of the array. For a periodic array, the total vortex potential is periodic with a fundamental lattice constant which is equal to the unit cell length. The results are shown in Figures 2.6 (a) and (b). The model is valid for a single vortex. Vortex-vortex interactions are not included.

In this limit, the predominant interaction of the vortex is with the underlying lattice. An applied bias current can tip this potential (similar to the washboard potential in phase space) and a critical current can be defined above which the local minima

disappear. This critical current is called the vortex depinning current and is proportional to the barrier height ($i_c^B = e\frac{E_B}{\hbar}$) for a purely sinusoidal potential, where E_B is the barrier height. Using the numerical result $E_B = 0.2\ E_J$, they find that $i_c^B = 0.1\ i_c$, where i_c is the single junction critical current.

This is the theoretically calculated value of the barrier height at zero or very low bias current. At temperatures way below the transition temperature, the vortices are trapped in the potential wells. For k_BT of the order of E_B, there is finite probability for thermal activation of the vortex.

2.5 The Resistive Transition in an Array

A large number of recent experimental and theoretical papers have been devoted to the superconducting to normal phase transition in two dimensions. The interest has been largely due to theoretical work [5,6,7] which noted that the Kosterlitz-Thouless [8,9] vortex unbinding picture of the transition which was originally applied to experiments on neutral superfluids, should apply to two-dimensional superconductors as well, provided that the transverse magnetic penetration depth $\lambda_\perp$ is larger than the sample width and length. The dissipation in Josephson junction arrays is attributed to vortex motion. A vortex encloses a magnetic field and a phase drop. Hence vortex motion is effectively the contribution of phase slips and the induced voltage due to rate of change of enclosed flux (Faraday's Law). At finite, non-zero temperatures, vortices have enough thermal energy to move around. Vortex motion can also be induced by external currents through the interaction of the current with the enclosed field (Lorentz force). The force on a vortex due to an external current $\vec{J}$ is given by the Lorentz force which is proportional to $\vec{J} \times \vec{\Phi}_0$. If the force is large enough to depin the vortex, then it results in dissipation. The

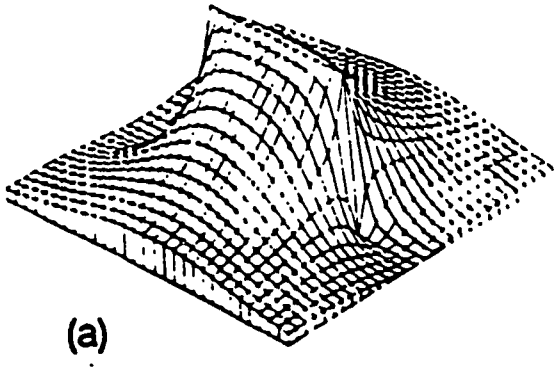

Fig: 2.6 (a) Vortex energy as a function of position on the junction. The energy is maximum when the vortex is on the junction.

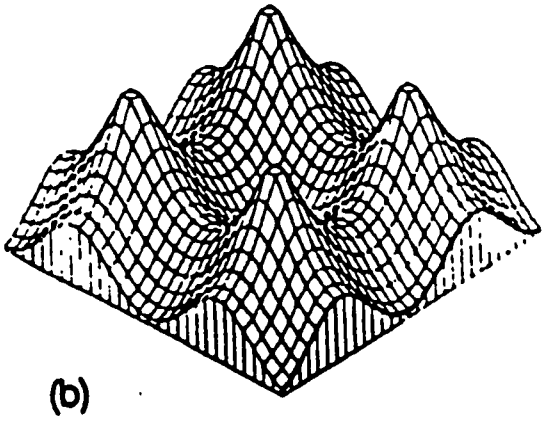

Fig: 2.6 (b) Vortex energy as a function of position on a 8 x 8 array. Energy is maximum when the vortex is on the island, minimum when it is at the center of the cell. The saddle point energy is when the vortex is on the junction

dissipation occurs through phase slips across the individual junctions. From the second Josephson relation, the phase slips result in an instantaneous voltage.

The resistive phase transition in thin films and arrays are largely governed by the motion of these vortices. Figure 2.7 is a plot of the resistive transition at zero field for a typical square Josephson junction array.[12] The transition has three distinct regions. The initial drop in resistance is at a temperature T_O. This is the temperature at which the islands go superconducting (this is usually the bulk transition temperature of the material which is 9 K for Nb). The onset of the second transition to a lower resistance takes place at T_{CO}. This defines the temperature below which the proximity effect between the superconducting islands (through the normal metal) becomes important. The phases of the junctions couple and the array is said to be in a phase-coherent state. This is indicated by the nonlinear, magnetic field dependent I-V characteristics. The coupling gets stronger as the temperature decreases and at a lower transition temperature T_C, the junctions couple causing the array to go into the superconducting state. T_C is identified as the Kosterlitz-Thouless (K-T) transition temperature. This is interpreted using the vortex picture of resistive transition.

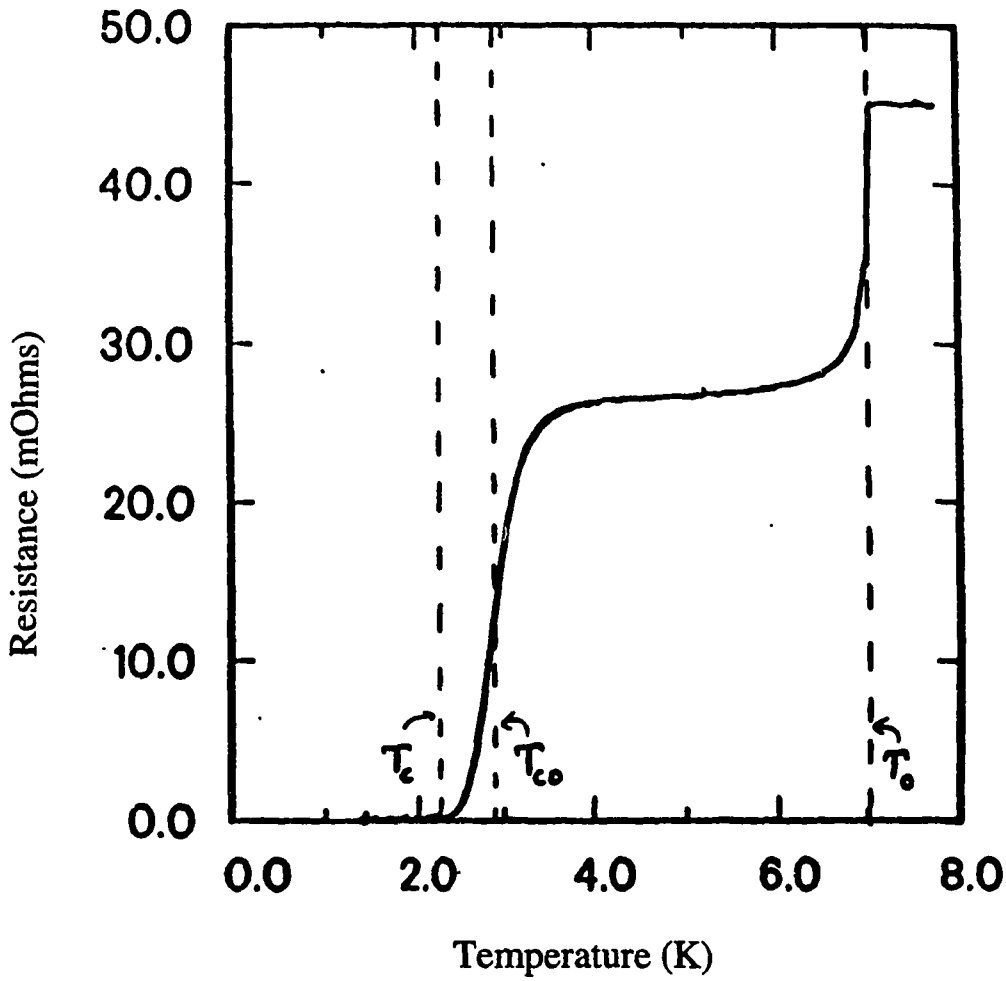

Fig: 2.7: The Resistive Transition of a Josephson Junction array

2.5.1 The Kosterlitz-Thouless Phase Transition

Kosterlitz and Thouless proposed a new type of order called topological order in two-dimensional systems where conventional long range order does not exist. The theory was originally applied to the XY model of magnetism, the solid-liquid transition, and the neutral superfluid.[8,13] The theory suggests that at finite temperatures, the energy to form vortex-antivortex pairs in a two-dimensional system is finite. Beasley et al [5] showed that a situation very similar to He films should arise in very thin superconducting films. This implies that for all temperatures above absolute zero, vortex-antivortex pairs should exist in a thin superconducting film. In a later experiment, Resnick and Garland[10] found that two-dimensional arrays of Josephson junctions also undergo the K-T transition.

The long range order in K-T systems is based on the overall properties of the system. The definition of long range order which we adopt arises naturally in the case of a solid from the dislocation theory of melting. The basis of this theory is that the interaction energy between vortex-antivortex (an antivortex is a quantized fluxoid with the field direction opposite to that of a vortex) pairs depends logarithmically on the separation between them up to characteristic distance $\lambda_{\perp}$. The energy to create a free vortex is also finite and in equilibrium a few vortices will exist along with the bound pairs. At the Kosterlitz-Thouless transition temperature T_c, the thermal energy becomes large enough to overcome the attractive interaction between the pairs. It is the dissociation of these pairs at T_c that marks the onset of the resistive transition. The free vortices screen the other pairs, thereby reducing the effective interaction and hence aiding the pair-breaking process. As the temperature increases above T_c, the number of free vortices increases and contributes to an increase in the resistance. In the region between T_c and T_{co}, the resistivity is thought to be due to the motion of these thermally activated

free vortices. A plot of ln (R/R_n) as a function of $(T_c/(T-T_c))^{1/2}$ is expected to be a straight line in this regime.

2.5.2 Flux Creep

Even at temperatures below T_c , it is possible to have a finite resistance through thermal activation of the free vortices. At sufficiently low temperatures and in zero field, the probability of free vortex creation is very small. This probability becomes significant only very close to the transition temperature. Free vortices can be externally induced by applying a weak magnetic field. For low magnetic fields, the vortices are spread far apart and vortex-vortex interaction can be ignored. In this limit, the pinning potential model discussed in Section 2.3, is valid. At temperatures way below T_c , these field induced vortices are tightly bound to the pinning potential of the array. As the temperature becomes comparable to the barrier height, it is possible for these field induced vortices to thermally activate out of the barriers resulting in a finite resistance. These free vortices increase the screening between pairs. This results in the onset of pair breaking at a lower temperature than the zero field T_c. The temperature dependence of the resistance is

$$R = R_o \exp(-E_B(T) / k_B T) \tag{2.12}$$

where $E_B(T)$ is the barrier height seen by the vortex due to the pinning potential of the array. This is usually proportional to the Josephson junction energy $E_J(T)$. If b is the constant of proportionality, then $E_B(T) = b\, E_J(T) = b \frac{\hbar i_c(T)}{2e}$. For an SNS junction close to the transition, the critical current $i_c(T) = i_{co}(1-T/T_c)^2$. Therefore, the resistance due to thermal activation can be rewritten as

$$R = R_0 \exp\{-\frac{b\,\hbar i_{co}}{2ek_BT}(1-\frac{T}{T_c})^2\} \qquad (2.13)$$

This gives a method for measuring the barrier height experimentally. The resistance R can be measured as a function of temperature T. A plot of log R as a function of $(1\text{-}T/T_c)^2$ should give a straight line with a slope which is proportional to the barrier height.

2.5.3 Flux flow

At temperatures above T_c, the barrier height of the pinning potential goes to zero and the vortices can move freely. This is defined as the flux flow regime. Flux flow can also be acheived below the critical temperature by applying an external current. If the Lorentz force due to the current is larger than the pinning force on the vortex, the vortices can flow freely. In this regime, the temperature dependence of the resistance is given by the Halperin-Nelson formula. [6,7]

$$R_0 \propto \exp\,[-A\,/\,(T - T_c)^{1/2}] \qquad (2.14)$$

This expression is valid at zero field and for small measuring currents for a continuous medium.

2.6 Equilibrium Vortex Configurations

Below T_c, the vortices are pinned to the array as discussed in Sec 2.4. For temperatures $T << T_c$ and for finite magnetic fields, the vortices arrange themselves in the lattice of the array such that the total energy of the system is minimized and the

system is in equilibrium. The minimum energy and the equilibrium configuration can be obtained from the Hamiltonian of the system.

For an array of junctions, the Hamiltonian is given by the sum of the coupling energies of the individual junctions

$$H = -E_J \sum_{ij} \cos \left(\phi_i - \phi_j - \frac{2e}{\hbar} \int \vec{A} \cdot \vec{dl} \right) \tag{2.15}$$

where the sum is over connected pairs of superconducting islands, counting each pair once. When the phase is zero or a multiple of 2π, the Hamiltonian reduces to the simple XY model. It describes an array of spins which make an angle ϕ_i with, say, the x-axis. When it is non-zero, vector potential term introduces frustration. We define a frustration parameter f which is a ratio of the applied flux to a flux quantum. Then the Hamiltonian can be rewritten as

$$H = - E_J \sum_{ij} \cos (\phi_i - \phi_j - 2\pi f)$$

It is important to point out here that the nature of the Hamiltonian brings out the symmetry in the problem between f and -f and also symmetry about f = 1/2.

In a Type II superconductor in the mixed phase, vortices prefer to align themselves so that the vortex-vortex repulsion is minimized. The equilibrium configuration with the minimum energy is the triangular lattice (Abrikosov). In an array, the magnetic field serves to induce an ordered lattice of vortices in the ground state. The vortices are constrained to lie at the pinning sites and thus uniform-film treatments are inappropriate. The periodic pinning potential of the array cannot be viewed as a weak

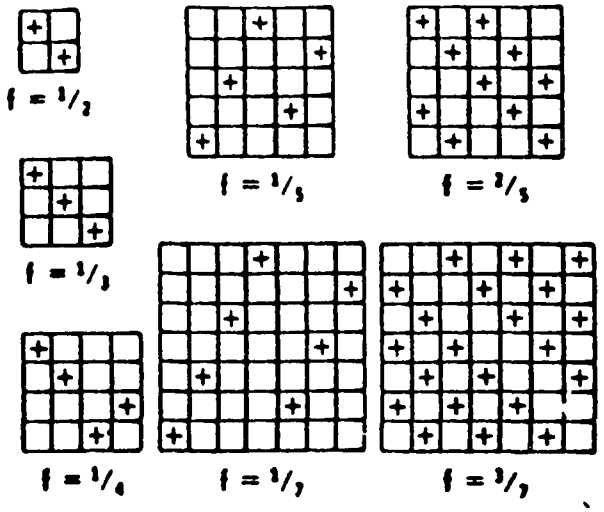

Fig: 2.8 (a)

Vortex configurations

for different values of f

where + is a vortex

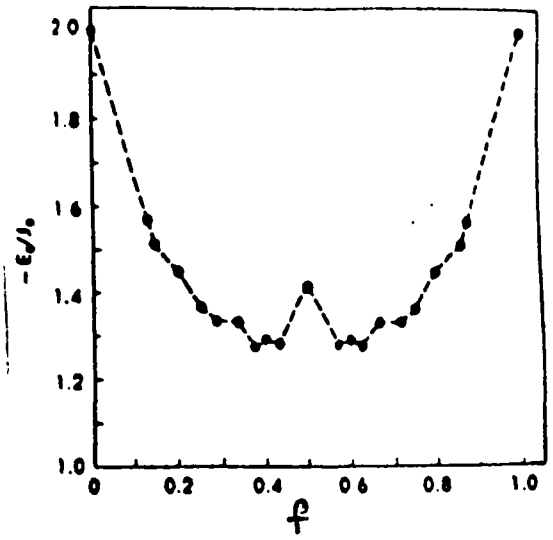

Fig: 2.8 (b)

Simulation of the energy

as a function of f

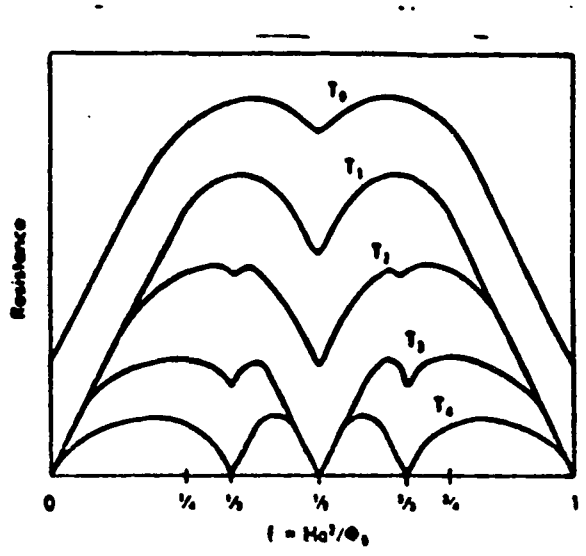

Fig: 2.8 (c) Simulation of the resistance as a function of field

perturbation on a uniform film. Detailed equilibrium calculations have been carried out for both f=0 and for low rational values of f. [8] The calculations are made using what is known as the XY model (for the f=0 case) and the frustrated XY model (for the finite f case).

2.6.1 Mean Field Calculations (XY model)

The two-dimensional XY model is a system of spins confined to rotate in the plane of the lattice. The interaction between neigboring spin vectors $\vec{s}_i$ and $\vec{s}_j$ summed over all the spins is given

$$H_o = -J \sum_{ij} \vec{s}_i \cdot \vec{s}_j = -J \sum_{ij} \cos(\phi_i - \phi_j) \tag{2.16}$$

The sum is over nearest neigbors only. The phase ϕ_i is the angle the ith spin makes with some arbitrary axis. It has been shown that this system does not have any long range order and that the ground state is unstable against spin -wave excitations. [9] Kosterlitz and Thouless have shown that in these systems, there exist metastable states corresponding to vortices which are closely bound in pairs below a certain critical temperature.

Expanding about a local minimum of H

$$H - E_o \approx \frac{1}{2} J \sum_{ij} (\phi_i - \phi_j)^2 = J \sum_{\vec{r}} (\Delta\phi(\vec{r}))^2 \tag{2.17}$$

where Δ denotes the first difference operator, $\phi(\vec{r})$ is a function defined over the lattice sites, and the sum is taken over all sites. Its energy is $H - E_o \approx \pi J \ln \frac{R}{a}$ where R is the radius of the system. This is a slowly varying configuration called a vortex, whose energy

increases logarithmically with size of the system. For some closed path around the center of the vortex, $\phi(\vec{r})$ will change by 2π for each revolution. Thus, for a configuration with no vortices, the phase will be single-valued, while for one with vortices, it will be many-valued.

The formalism which has been used for the spin systems can be applied to arrays since the spin system Hamiltonian is similar to the H for arrays (eqn. 2.15). A vortex in a Josephson junction array can be defined in a similar way. Teitel and Jayaprakash [8] use the uniformly frustrated XY model to calculate the ground state vortex configurations. They studied the T=0 properties of the Hamiltonian by doing Monte Carlo simulations on q x q lattices with periodic boundary conditions. The simulation determines the position of the vortices for different values of f as shown in Fig: 2.8 (a). The vortices try to maximize their distance from each other to achieve minimum energy. This gives rise to a vortex pattern in the array which is commensurate with the array lattice. The energy is obtained by symmetry arguments applied to the phase differences across the bonds as shown in Figure 2.8 (b). Note that the energy is periodic in f and symmetric about f=1/2. An f of p/q per cell corresponds to p vortices for every q cells in the array. Hence for any unit of q cells in the array, the net circulating currents are minimized. The resistance as a function of field for the array is also predicted using Monte Carlo simulations, for different temperatures. The results are summarized in Figure 2.8 (c).

REFERENCES

1) For a review of the field, see Proceedings of the NATO Workshop on Phase Coherence in Superconductor Networks, edited by J. E. Mooij and Sch on, Physica B **152** (1988)

2) B. D. Josephson, Phys. Lett. **1**, 251 (1962)

3) W. C. Stewart , Applied Physics Letters, **12**, 277 (1969)

4) D. E. McCumber , J. Appl. Phys. **39**, 3113 (1968)

5) M. R. Beasley, J. E. Mooij, and T. P. Orlando, Phys. Rev. Lett. **42**, 1165 (1979)

6) B. I. Halperin and David R. Nelson, J. Low Temp. Phys. **36,** 1165 (1979)

7) S. Doniach and B. A. Huberman, Phys. Rev. Lett. **42,** 1169 (1979))

8) S. Teitel and C. Jayaprakash, Phys. Rev. B **27**, 598 (1983); Phys. Rev. Lett. **51**, 1999 (1983);
W. Y. Shih and D. Stroud, Phys. Rev. B **32**, 158 (1985);
Ying-Hong Li and S. Teitel, Phys. Rev. Lett **65**, 2595 (1990);

9) J. M. Kosterlitz and D. J. Thouless, J. Phys. C **6**, 1181 (1973)

10) J. M. Kosterlitz, J. Phys. C **7**, 1046 (1974)

11) D. J. Resnick and J. C. Garland, Phys. Rev. Lett **47**, 1542 (1981)

12) A review on KT transition in thin films and Josephson junction arrays can be found in J. E. Mooij, in NATO *Advanced Study Institute on Advances in Superconductivity*, edited by B. Deaver and J. Ruvalds (Plenum, New York, 1983), p.433

CHAPTER 3

EFFECTS OF INTRINSIC DISORDER ON TRANSPORT MEASUREMENTS IN LARGE JOSEPHSON JUNCTION ARRAYS

Phase transitions in low dimensional systems have been of interest to theorists for over two decades now.[1] The dimensionality of these systems determines the nature of the ordering. In the search for suitable systems to test these ideas, granular superconducting films have been used.[2,3] However, it is difficult to make thin, homogenous films. The films have inherent disorder which cannot be controlled. Improvement in microfabrication technology has made it possible to make model systems for superconducting thin films with controllable parameters. These are the two-dimensional Josephson junction arrays which were discussed in detail in Chapter 2.[4] It is known that at f=0, they exhibit a K-T like phase transition due to the depairing of thermally activated vortex-antivortex pairs. For non-zero, finite f, the nature of the transition is not fully understood. At low fields (f=0 to 0.15), it is thought to be due to thermal activation of field induced vortices. At higher fields, it is thought to be due to a combination of depairing and domain formation much like in magnetic systems.

In this Chapter, we start by describing the sample fabrication techniques and the experimental set-up. Then we present the results of transport measurements on large square arrays of Josephson junctions. The effect of disorder on both the resistive transition and the magnetoresistance is discussed. The resistive transition data shows structure close to the transition which can be interpreted in terms of a non-uniform spread in the critical temperature of regions in the array. The substructures in the magnetoresistance tend to wash out with disorder though the periodicity of f=1 is maintained.

The theory of the resistive transition is well understood for small bias currents. As the bias current is increased, the pinning potential for the vortices decreases. The system moves away from equilibrium. Measurements of the resistive transition have been made for different bias currents to look for this shift to non-equilibrium.

3.1 Sample Fabrication

The Josephson Junction arrays are fabricated using a two-step photolithographic process. Photolithography is the process by which a substrate coated with a light sensitive polymer (photoresist (PR)) is exposed to light through an optical mask used to define the device pattern. The optical mask is a glass plate coated with a metal (usually Cr) in which a pattern has been etched. The resolution of this process is limited by the wavelength of the light used and diffraction effects.

Ultraviolet (u-v) light at a wavelength of approximately 320 nm is used. Depending on the resist thickness, exposure times may range from 30 sec to 90 sec at an intensity of about 12 mW/cm^2. The substrate is then soaked in a developer solution. The developer is a base consisting of NaOH or KOH diluted with deionized water. This solution attacks the whole resist, but removes the U-V exposed areas at a much faster rate. Typical developing times are of the order of 10-30 sec.

The resolution (smallest feature) that can be patterned with optical lithography is about 1μm. This limit is due to diffraction effects from the edge of the mask pattern and the thickness of the resist. It is possible to obtain smaller resolution using thinned resists and ensuring good contact between the substrate and the mask. However, the process is very laborious and it is easier to use electron beam lithography.

We have made arrays using either Pb or Nb for the superconductor and Cu or Al for the normal metal. These are deposited as thin films on silicon substrates. The

deposition method depends on the element used. Lead and copper are evaporated and Nb and Al are sputtered for best results. Lead undergoes a superconducting transition at 7 K and Niobium at 9 K. Lead has a low melting point and is easy to evaporate. The evaporation rate is about 30-80 Å/sec. The major disadvantage of using Pb-based devices is the poor quality of the Pb films. Evaporated Pb films have an FCC crystal structure which in thin films is mechanically unstable. It has a tendency to form hillocks. The film is also not rugged and will scratch off easily during handling. During the two-step fabrication process, the sample has to be baked at high temperature. Above about 70°C, lead film becomes unstable and forms grains. It also has a great affinity for oxygen and the film will oxidize completely through if exposed to air for a few days. The quality of the film also degrades with thermal recycling, either during resist bakes or cryogenic cooling. Therefore the sample cannot be used many times due to lack of reproducibility. Additionally, standard photoresist developers etch lead.

Most of these problems can be solved by using niobium instead of lead. It can handle high bake temperatures and thermal recycling. When exposed to air, the surface oxidizes and protects the underlying layers. The difficulty in using Niobium is that it is not easy to obtain high quality, pure films. Evaporated Nb films usually have large tensile stress which is difficult to control. So dc or rf sputtering is the other choice. Niobium has a tendency to getter oxygen and is extremely sensitive to other impurities. Therefore, sputtering at very low base pressures in a Nb dedicated system is necessary to ensure quality and reproducibility. There are also problems related to Nb film stress. The stress of the films varies from compressive to tensile depending on sputtering conditions. At low Ar pressure, the stress is tensile and changes to compressive as the pressure increases. If film adhesion to the substrate is poor, the tensile stress causes the

film to tear apart during liftoff. If it is compressive, the liftoff procedure causes the film to buckle under pressure. Our Nb films are obtained from a cryo-pumped deposition system where the base pressure is maintained in the high 10^{-8} to mid 10^{-7} torr range. The cryopump is a Torrmaster TM150 from CVI Incorporated. It has a integral closed cycle Gifford-McMahon type refrigerator. The deposition chamber is a bell jar type structure with a load-locked chamber for loading the samples. There are four sample holders, two 2" dc sputtering targets (Nb and Al targets from Pure Tech) and one rf sputtering gun for SiO_2. A base pressure of less than 4×10^{-7} torr is necessary for high quality Nb. A 1" ion mill incorporated inside the chamber. This is used to clean the substrate by exposing it to a Ar ion beam current of 10 mA for 30 sec. The typical beam voltage used is 400 V. This removes the oxides on the surface and also helps improve film adhesion to the substrate. The target is also presputtered for a minute to get rid of contaminants that might be on the surface. The Nb is sputtered in a partial Ar pressure of 10 mtorr. A deposition rate of 20 Å/sec is found to be optimal for good low stress Niobium films. A crystal thickness monitor (Inficon - XTC) is used to measure the film thickness in-situ.

Copper, with its high conductivity, is the best candidate for the normal metal. The coherence length in the normal metal (which is one of the factors that affect the proximity effect) is dependent on conductivity (and hence the purity) of the metal. Copper is typically evaporated in a conventional evaporation system with base pressures of the order of 2×10^{-6} Torr. We use a bell jar evaporation system from Davis and Wilder Inc. Vacuum is achieved using a diffusion pump with a cold trap. This system is also fitted with a 1" ion mill (Ion Tech Inc.) for cleaning the substrates prior to evaporation.

Aluminum can also be used in place of Copper for measurement temperatures above 2 K. It undergoes a superconducting transition at about 1.4 K and its resistance becomes temperature dependent below 2 K. The substrates are thin, polished Si wafers.

Fig: 3.2. The 2 step Array Fabrication Process

Polished quartz or glass substrates can also be used. All the lithography is done in a Class 1000 clean room with Class 100 under the flow benches.

The actual steps in the sample fabrication process are as follows:

1) In Figure 3.2, the process is pictorially represented. We start by defining the network lines (in a criss-cross pattern). This is done by spinning 0.8 μm of 1350 J PR onto the Si substrate. The PR is pre-baked in a 90^{o}C oven for 20-30 minutes to evaporate the solvents and harden the resist. This improves the resolution. The substrate is then mounted on the optical aligner and exposed to ultra-violet light through a contact mask. The exposed regions of the PR are then developed away using 351K developer. The lines thus formed are 2μm wide. After developing, it is important to clean the substrate with deionized water and spin dry. Post baking at 90^{o}C for 5 minutes is recommended.

Occasionally, there might be problems with respect to adhesion of PR on the Si substrate. This can be avoided by exposing the substrate to HMDS (hexa-methyl-di silazane) vapor in the fume hood before spinning the PR. This improves the Si surface properties for resist adhesion.

2) Then copper/aluminum and niobium/lead are sequentially deposited onto the substrate in that order. Before deposition, the substrate is cleaned using the ion mill. This removes surface oxides. The ion mill is incorporated in both the sputtering system and the evaporator. We use a 1" ion mill (Ion Tech) and a 10mA/cm^2 beam current at a voltage of 500 V for 15 sec. Copper is evaporated at a rate of 10 /sec after the evaporator is down to a base pressure of 2 x 10^{-6} Torr. The thickness of the normal metal deposited is about 2000 Å. If Pb is the superconductor used, then 1000 Å of Pb is sequentially evaporated on Cu without breaking the vacuum in the evaporation chamber. This ensures a good Pb-Cu interface. In the case of Nb-Cu devices, there is no choice but to expose the Cu film to atmosphere since Nb has to be sputtered. The Cu surface is cleaned using

the ion mill in the sputtering chamber before depositing 1200 Å of Nb. The superconducting lines are obtained using a lift-off procedure. This is a process by which the resist stencil along with the metal, is dissolved following thin film deposition, by soaking the sample in acetone. Liftoff can be accelerated using ultrasound.

3) The next step is to pattern the S-N-S gap. PR is once again spun on the sample and exposed through the mask. The gap width is typically about 1.3μm.

4) The superconducting material in the "gap" is removed using ion beam etching or reactive ion etching. It is important to use a technique which will remove the superconductor but barely affect the underlying normal metal. In the case of a Pb-Cu-Pb array, the lead is ion milled using a 1" collimated ion beam and a beam current of 10 mA. The milling rate for Copper is about five times less than that for lead and hence is not affected much. Niobium is resistant to ion milling and we have to resort to reactive ion etching (RIE) using a CF_4 plasma. We use an R.D. Mathis Model SP430 Radio Frequency Glow Discharge Sputtering system for RIE. It consists of a 13.56 MHz r.f. generator, coupling unit and deposition chamber. The typical etching times are around 8 minutes for a 1100 Å in a 100 mTorr pressure of CF_4. During RIE, the rf field in the chamber causes the CF_4 molecules to break up into CF^3 and F^- and other radicals. The fluorine ion reacts with the Nb and forms gaseous molecules which are then pumped out of the system. RIE is a good technique for getting clean and well defined gaps because it is very directional. RIE in pure CF_4 results in polymer build up along the side walls of the PR. Both copper and aluminum are resistant to plasma etching.

3.2 Experimental Setup

The measurements are conducted in a pumped He^4 bath cryostat. A pictorial representation of the insert is shown in Figure 3.3. The sample is mounted on a 1.75"

Copper mount which is anchored via a threaded joint to the Copper base of a He^3 pot. There is provision for heating the sample using a non-inductively bound heater wire which is wound to the base of the He^3 pot. The thermometer is also mounted on the base of the pot. Temperatures as low as 1.3 K can be reached by pumping on the Liquid He using a rotary blower pump backed by a large mechanical pump.

The sample is normally isolated from the He^4 bath by two brass vacuum cans sealed with Indium O-rings. Thermal isolation from the bath can be achieved by completely evacuating the outer can. The temperature of the outer can wall is at the temperature of the liquid He bath. A small amount of Helium exchange gas can be added into the vacuum can to adjust the thermal linkage between the bath and the sample. The thermometer used is a Lake Shore Cryotronics Inc., Germanium thermometer (GR-200A-100). Its operating range is from 1 K to 4.2 K.

A Helmholtz coil (detachable) which slips over and attaches to the sample mount is used to apply a uniform magnetic field, perpendicular to the sample. The two sets of Helmholtz pairs are wound on a 2" phenolic sleeve such that the parallel midplane of the pairs is set at about a substrate's thickness above the surface of the sample mount. The primary pair consists of 150 turns each, of superconducting Nb-Ti 4mil wire wound into 1/8" square grooves. This provides a uniform field with a maximum deviation of 0.01 % over 1/8 its diameter, 0.18% over 1/4, and 3.3% over 1/2, with rapid degradation over larger areas.

Because of the sensitive nature of these experiments, stray magnetic fields are a real concern. The typical cell size in our arrays are $20\mu m \times 20\mu m$. One flux quantum ($2.07 \times 10^{-7} G\ cm^2$) in the cell corresponds to a field of 0.05 Gauss. This is one tenth of the earth's magnetic field of 0.5 G. So a double mu-metal shield is used to enclose the dewar. The field inside a single sheet of mu metal falls off as μ^{-1} where μ is the

Fig: 3.3 Cryogenic insert for cooling down and measurement of samples

permeability of the metal. Consequently, a double mu metal shield will reduce the earth's field to 1 mG or less. For regions close to the sample on the insert, the measured field (with the mu-metal shield on) was negligible. A superconducting lead bag around the outer vacuum can, helps to exclude magnetic field through the Meissner effect.
The other source of noise is electromagnetic fields (especially high frequencies). To reduce rf noise, the cryostat is placed within an rf-shielded room. Batteries are used as much as possible to reduce 60 Hz generation and pickup within the room. Output signals are typically buffered by a preamp before being passed via coaxial feedthroughs to the computer data acquisition system outside the room. We use a Model 300 x SQUID probe from S.H.E corporation which has a Model 300 rf head and a Model 30 control unit along with a model SP magnetometer SQUID probe. This is a hybrid (thin film) SQUID sensor. A small shunt resistor is usually installed across the input terminals. This in parallel with a 2 μH signal coil forms a low pass filter. The hybrid is contained in a hermetically sealed package. The rf bias frequency is 19 MHz.

Limit of sensitivity of an rf SQUID increases with increasing frequency. The expected limiting sensitivity for a 1 Hz bandwidth (for the typical value of L=1nH and $\omega = 2x10^{-8}$ Hz) is $\delta\Phi / \Phi_0 = 2x10^{-5}$.

3.3 Transport Measurements

Transport data involves the measurement of the voltage and the resistance of a sample as a function of a parameter, keeping all others fixed. Measurement of the resistance as a function of temperature for a fixed current bias and constant magnetic field gives information about vortex-antivortex interaction and the interaction of the vortex with the array lattice potential as a function of thermal energy. All the measurements

presented here have been made on a 500 x 500 square array. The data is presented for different values of bias current and applied magnetic field. The bias current affects the Lorentz force on the vortex. The external field induces additional vortices which screen the vortex-antivortex interaction and lower the resistive transition temperature.

The measurement of voltage as a function of external magnetic field for a fixed bias current and temperature is also of interest. The variation of voltage with field mimics the variation of energy with field. In Section 2.6, the equilibrium vortex configurations were shown for different values of field. The energy was shown to be periodic in the field with a period of a flux quantum with substructures at f=p/q (p, q being integers) which correspond to vortex configurations that are commensurate with the underlying vortex lattice. The measured voltage across the sample also shows periodic variation with field and minima at f=p/q. The number of minima gives information about the extent of the long range phase coherence across the array. As the bias current is increased, the voltage increases and the minima at lower values of f (and higher values of 1-f) disappear.

Figure 3.4(a) is a plot of the voltage vs flux for a 500 x 500 square array (Nb-Cu-Nb) for three different bias currents. The voltage is periodic in the magnetic field f (per unit cell). There are three minima at f=1/3, 1/2 and 2/3. No substructure is seen for other commensurate values of f. This implies that the phase coherence does not extend beyond about nine cells. This is probably due to intrinsic bond disorder during fabrication. For low fields, the voltage (and hence the resistance) is linear with field. This is the regime where the vortex-vortex interaction is still minimal and pinning of the vortices with the underlying lattice plays the dominant role. The resistance at zero field as a function of temperature is shown in Figure 3.4(b) for a square 500 x 500 array for three different values of f. As the field is increased from 0 to 0.1 and 0.2, the critical temperature is suppressed as expected. This is due to the presence of field induced vortices that

Fig: 3.4 (a) Voltage vs. flux for a Nb-Al-Nb array at T = current biases of (b) (b) Resistance vs. temperature for f = 0, 0.1 and 0.2

screen the vortex-antivortex pairs and induce depairing at a lower temperature. The V vs. f plot is smooth and symmetric about f =1/2 but the resistive transition shows structure close to the transition temperature. This is unlike the R vs. T plot of Fig: 2.7. The structure in the resistive transition of our data might be ue to array non-uniformity.

3.3.1 Effect of array non-uniformity on the resistive transition

Figure 3.5(a) is a plot of the resistance vs. temperature, very close to the transition for a 500 x 500 square array. Three onsets are observed in the temperature range from 1.08 K and 1.18 K for a bias current of 34 mA at f = 0 and f = 0.03. Similar structure is also seen at a lower bias current of 25 mA. The shape of the onsets suggests a possible superposition of three regions, each having a slightly different T_c (1.11 K, 1.12 K, and 1.125 K). Figure 3.5(b) is a simulation of a resistance curve where the resistance due to three different transitions have been superposed. We assume that the resistance, to the simplest approximation, varies as

$$R \propto b * \exp\left(a / \left(T / T_c\right)\right) \quad \text{for } T > T_c$$

where a is an arbitrary constant. The resistance due to the superposition of three regions having different transition temperatures,

$$R = \sum_i R_i \quad \text{where} \quad R_i \propto \exp(a / (T / T_{ci}))$$

The curve in Figure 3.5 (b) is obtained using the above formula for three different transition temperatures. There is a good qualitative fit between the simulation and the data at a bias current of 25 mA indicating that a spread in critical temperatures could be a likely cause for the structure in the resistive transition.

The non-uniformity in the critical temperature in this sample is due to non-uniformity in the critical currents. A direct correlation can be made between the steps in the resistive transition and the degree of disorder. Greatee the number of steps, the greater

is the degree of disorder. The resistive transition is therefore a good tool for studying non-random disorder. The critical temperatures can also be related to the barrier heights. The array provides a periodic potential energy of pinning sites for vortices and the barrier height is proportional to the critical current.

Similar structures in the resistive transition, have been observed some of the other samples that we have measured. Analysis of the disorder in terms of a spatial spread in the critical currents of the sample is however complicated because it involves solving the dynamical equations of 500 x 500 junctions in a specific configuration. The simple simulation in Figure 3.5(b) only gives a qualitative idea and a clue towards the cause of the disorder. A better understanding of the local effect of critical current defects in arrays, can be obtained by studying smaller samples. This is discussed in detail in Chapter 4.

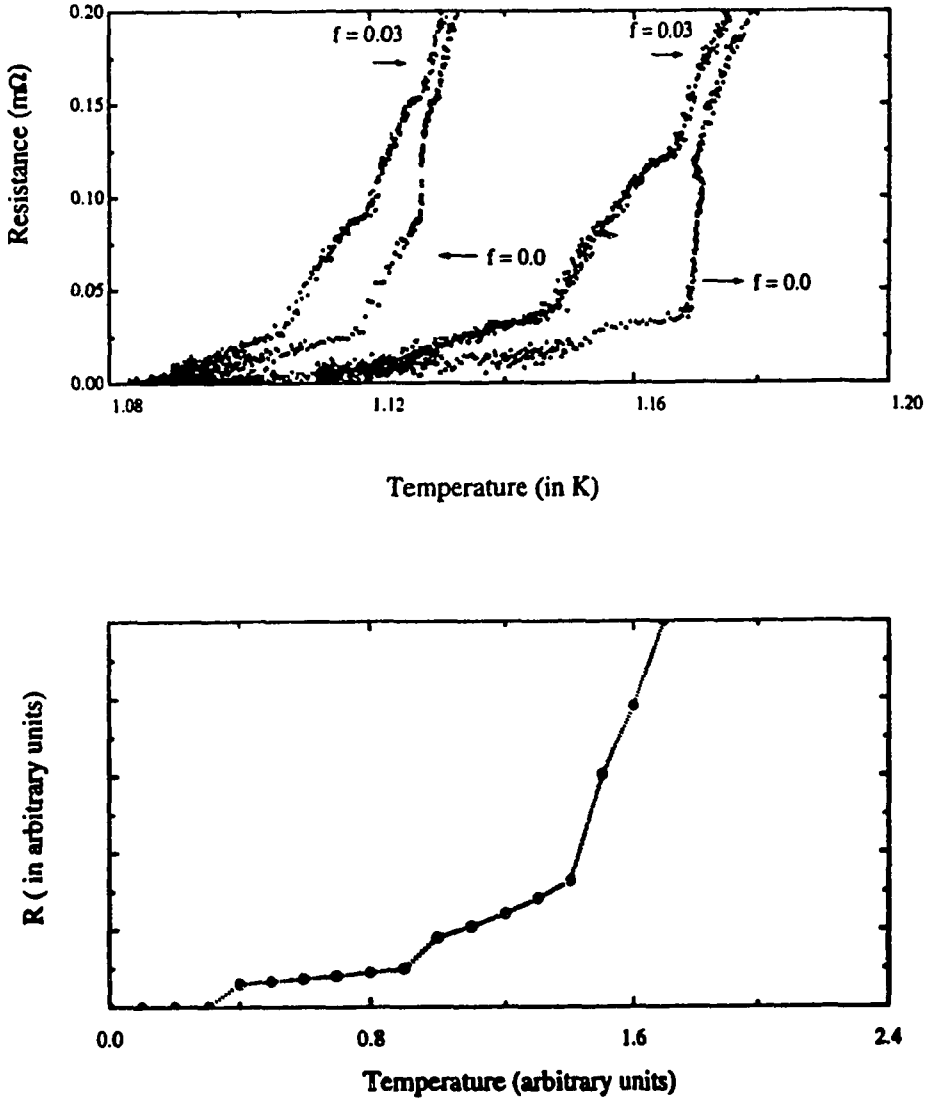

Fig: 3.5 (a) Features in the resistance, close to the transition temperature

(b) Simulation of the resistive transition for a spread in the critical current

3.3.2 The broadening of the resistive transition for small magnetic fields.

Effect of small ($f < 0.1$, where the voltage reponse to field is linear) magnetic fields has been of recent interest with respect to the vortex pinning model described in Chapter 2. This model is valid for low bias currents and in the regime where the vortex-vortex interaction is weak. Experimentally, this is acheived by applying small fields which results in a vortex distribution that is well spaced out. The field induced vortices are mobile even below the transition temperature, because the barrier height is $0.2\ E_J$ ($E_J = k_B T_c$) and this results in a finite resistance. Application of small magnetic fields should result in a dramatic broadening of the resistive transition. Rzchowski et al [9] have observed this broadening in their array samples.

We have done similar measurements at low fields to study the effect that the intrinsic disorder has on the vortex pinning. In Fig: 3.6 (a) the broadening of the resistive transition is shown for $I_b = 25\ \mu A$ bias currents as the field is increased from $f = 0$ to $f = 0.05$. There is significant broadening of the resistance as the field is increased from $f = 0$ to $f = 0.01$ which corresponds to a vortex every 100 cells. Increasing the field to $f = 0.03$ (every 33^{rd} cell) and then to $f=0.05$ (every 20th cell) causes only a small broadening at the first resistive onset. There is no visible broadening for increase in field from $f=0.05$ (vortex in every 20th cell) to $f=0.5$ (vortex in every alternate cell) as shown in Fig: 3.6 (b). It is possible that for fields greater than $f=0.05$, the vortex-vortex interaction becomes significant. It becomes more difficult for individual vortices to thermally activate out of the barrier due to the coupling with other vortices. Therefore study of small field broadening gives information about the crossover from weakly interacting, thermally activated vortices to strongly interacting vortex lattice.

Fig: 3.6 Broadening of the resistive transition

3.3.3 Measurements of the resistance as a function of temperature for different bias currents.

The previous measurements have reflected the effect that an applied magnetic field has on the resistive transition. Another parameter that influences the transition dramatically is the bias current.

Figure 3.7 (a) is a plot of R vs T for different values of bias current for a 500 x 500 square array. The critical temperature decreases as the bias current is increased from 1μA to 5μA. The bias current applies a Lorentz force on the vortices and causes the vortices to depin at a lower temperature. The inset is a blowup of the resistive transition over a small temperature range (1.45 K to 1.55K). Structure similar to that in Figure 3.6 is also observed in this sample for the lower bias currents.

The mechanism of the transition depends on the bias current. At lower bias currents, the dominant mechanism for vortex motion is expected to be thermal activation from the pinning sites. As the current is increased, the dominant mechanism is expected to be flux flow because the current causes a lowering of the barrier heights (this is the spatial equivalent of the washboard potential in phase space in Figure 2.3 (b)).

To check for thermal activation, log R is plotted as a function of $\frac{1}{T}(1-(\frac{T}{T_c})^2)$ in Figure 3.7(b). If this is linear (Sec 2.5.2), the slope should give the barrier height as a function of the Josephson coupling energy. The plots are linear over the temperature range close to the transition (1.45 K to 1.6 K). The slope at I_b = 1 μA gives a value $[i_c(T=0)*\frac{E_B}{E_J}]$ = 2.19 μA where $i_c(T=0)$ is the single junction critical current at T=0. For the expected barrier height of 0.2 E_J, this gives a very high zero temperature critical current of 0.22 mA. The slope, however does decrease for increasing bias currents implying that the barrier heights decrease with increasing bias current.

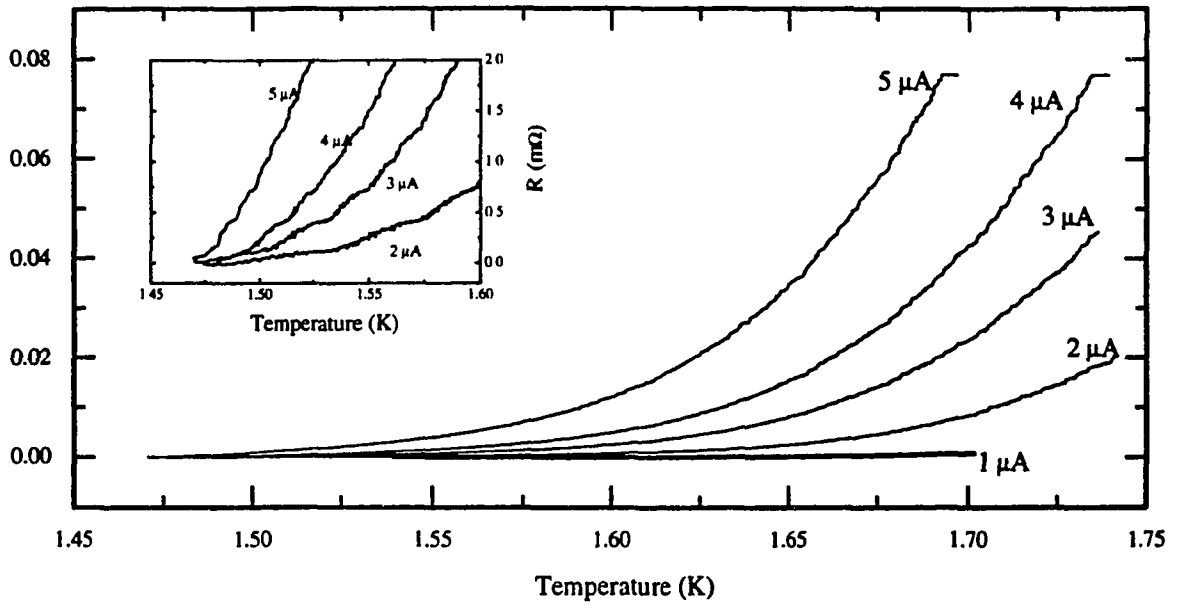

Fig: 3.7 (a) Resistance vs. Temperature
for different bias currents

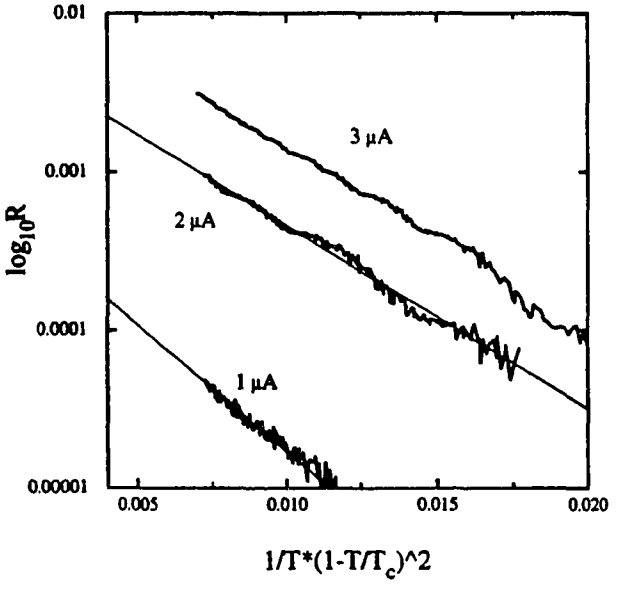

Fig: 3.7 (b) Thermal Activation model

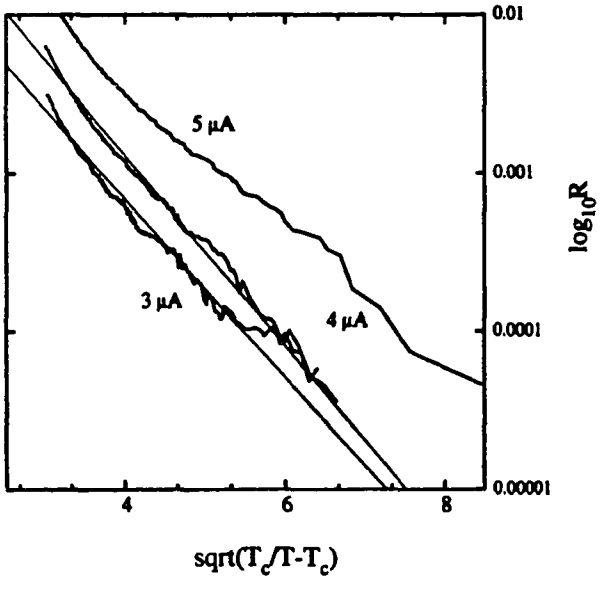

Fig: 3.7 (c) The Flux Flow model

Figure 3.7(c) is a plot of the data using the flux flow model (Sec 2.5.3). The plots for the higher bias currents (4μA and 5μA) show a linear slope indicating the possibility that the vortices are in the flux flow regime.

3.4 Conclusion

We have done transport measurements on 500 x 500 square arrays. The resistance of the array close to the transition temperature and for small magnetic fields is a useful tool for studying the effects of disorder and the extent of vortex-vortex interaction.

The resistive transition data shows a series of substructures close to the critical temperature. We have interpreted this by assuming that there are regions of the array that have slightly different transition temperatures. The spread in the critical temperatures is indicative of a spread in the critical currents of the junctions which arises due to variations in the S-N-S gaps of the junctions. A better understanding of intrinsic disorder can be obtained by doing measurements of small Josephson junction arrays.

. It is to be noted here that the analysis is by no means exhaustive or complete. Large arrays are useful model systems for thin film superconductors but they are extremely complex to analyze.

REFERENCES

1) J. M. Kosterlitz and D. J. Thouless, J. Phys. C **6**,1181 (1973); J. M. Kosterlitz, J. Phys. C **7**, 1046 (1974)

2) B. I. Halperin and D. R. Nelson, J. Low Temp. Phys. **36**, 599 (1979); M. Beasley, J. Mooij, and T. Orlando, Phys. Rev. Lett. **42**, 1165 (1979); S. Doniach and B. A. Huberman, Phys. Rev. Lett. **42**, 1169 (1979)

3) A. F. Hebard, and A. T. Fiory, Phys. Rev. Lett **44**, 291 (1980); A. F. Hebard and J. M. van den Berg, Phys. Rev. Lett. **44**, 50 (1980)

4) A review on KT transition in thin films and Josephson junction arrays can be found in J. E. Mooij, in NATO *Advanced Study Institute on Advances in Superconductivity*, edited by B. Deaver and J. Ruvalds (Plenum, New York, 1983), p.433.

4) D. J. Resnick and J. C. Garland, Phys. Rev. Lett **47**, 1542 (1981).

5) S. Doniach and B. A. Huberman, Phys. Rev. Lett. **42**, 1169 (1979).

6) Richard F. Voss and Richard A. Webb, Phys. Rev. B **25**, 3446 (1982).

7) M. Tinkham, David W. Abraham, and C. J. Lobb, Phys. Rev. B **28**, 6578 (1983).

9) M. S. Rzchowski, S. P. Benz, M. Tinkham, and C. J. Lobb, Phys. Rev. B **42**, 2041

CHAPTER 4

CLUSTERS

In a uniform Josephson junction array, phase coherence exists over many identical junctions (long range ordering). However, if there is non-uniformity of either the junction critical currents, or cell areas, or if there are missing junctions, then this long range order is destroyed. In these disordered systems, there are local regions where short range order exists. The phase coherence between the regions is weak or non-existent and the features in the magnetoresistance are washed out. The local properties of the vortices is different from that in large arrays. An appropriate model system to study this effect is a small Josephson junction array. We refer to such arrays (typically less than 5x5) as clusters. A cluster is a mesoscopic system which is large enough to exhibit phase coherence and vortex interactions present in large arrays, but small enough that disorder and discrete vortex motion are not averaged out. Because of the relatively few junctions in clusters, we can perform computer simulations of the Josephson phase dynamics and compare them directly to measurements that probe vortex motion. Such microscopic simulations are not feasible in large arrays.

Previous studies of small arrays include work on dc SQUIDs,[1] three junction interferometers,[2] single rings containing three or more junctions,[3] and linear arrays of coupled junctions.[4,5,6] Simulations of the I-V characteristics and the rf effects for small arrays with and without disorder has been of recent interest.[7,8,9]

We present transport measurements and the static and dynamical computer simulations of clusters. These simulations have been made from first principle calculations using the Josephson relations for each junction, the flux quantization for each loop, and the current conservation at each node. The programs to calculate the energy as

a function of flux and the voltage as a function of flux were originally written by Dr. K. Springer (an earlier student). The basic geometry of a 2x2 cluster is as shown in Figure 4.1. The simulations are based on this geometry.

4.1 Theory

Each Josephson junction of an array has a phase associated with it and in this phase space, the dynamics of the junction can be described using the washboard potential as discussed in Chapter 3. Therefore an array with N junctions can be completely described by a washboard potential in N-dimensional phase space. The dynamics of the system can be obtained by solving for the dynamics of each junction and including the current conservation and flux quantization requirements. In a large array with hundreds of junctions, the large amount of computation time required makes this technique inefficient. This procedure can however be used to obtain both the static and the dynamic properties of the clusters which consist of relatively few junctions.

4.2 Static properties

The static properties of interest are the total energy of the system, the equilibrium vortex configurations for different applied magnetic fields, the spatial cluster potential for vortex motion and the barrier heights to motion.

The total energy of the system is defined by the Hamiltonian in Chapter 2, equation 2.10 and is essentially the sum of the Josephson energies of the single junctions. An M x N array is defined as one with M columns and N rows. The current is injected and removed through the two superconducting bus bars at either end of the array. Each arm of the cell has a junction so that all the cells away from the edge of the array

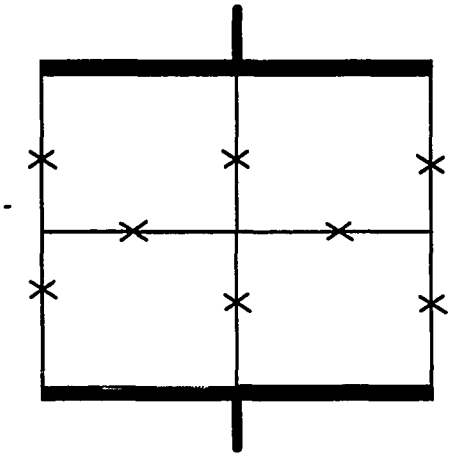

× represents a weak link

Fig: 4.1 The 2x2 cluster geometry

have four junctions. The cells at the edges have three junctions each. Each superconducting island has a phase ϕ_i associated with it. Only nearest neighbor interactions are included in the Hamiltonian. To first order, in the absence of any applied field, the energy of the cluster is just equal to the sum of the Josephson energies of all the junctions. An external applied field introduces additional phase factors in the Hamiltonian.

Various quantities are normalized to simplify the simulations. The circulating currents and the bias current are normalized to I_c. The inductance per link is given by $\beta_J = (2\pi L_J I_c) / \Phi_o$, so that when multiplied by a normalized current, it gives the internally generated flux directly as a phase contribution. Similarly, the externally applied flux is converted to a phase contribution by normalizing to $\Phi_o / 2\pi$. Finally, voltages are expressed in units of I_cR, while dimensionless time is given by $\tau = t / (\Phi_o / 2\pi I_c R)$. The Josephson equations for each junction, along with the current conservation and flux quantization requirements are then used to obtain the energy of the cluster as a function of flux.

1) The cluster parameters in the program like the array width and length, the loop inductance (normalized to β), the bias current per junction, the Josephson coupling energy for each junction, and the cell areas are set externally. The program involves dynamic evolution of the junction phases. The specifics of the phase evolution with time, like the time steps, the time interval between steps are external input parameters . This control over the individual parameters of the junctions and cell areas, enables us to control the extent of non-uniformity in the cluster. Disorder can be either random (linear or logarithmic spread in the critical currents or cell areas) or bond (cell) specific.

2) The junction inductance is set equal to a quarter of the loop inductance. Given the inductance of each junction, the first step is to calculate the inductance matrix of the

cluster. The diagonal elements are the self inductance of the loops and the non-diagonal elements correspond to the mutual inductance between loops. Only nearest neighbor interactions are considered. The inverse inductance matrix is then obtained using a standard subroutine.

3) The metastable energy at each value of flux is the sum of the individual junction energies ($E_c = E_J \cos\phi_{ij}$ where ($\phi_{ij} = \phi_i - \phi_j$)) for zero bias current. We start by setting the initial phase drops randomly. This does not give the metastable energy state of the cluster because it does not include the flux quantization requirement. For any given value of applied field, the first step involves finding out if the sum of the phases equals the total flux enclosed.

Is (sum of the phases around the loop) = - (total flux enclosed in that loop) ?
If this condition is not satisfied by the external flux, then circulating currents are generated to satisfy the quantization requirement. The flux in the i^{th} loop from circulating currents J_j in the junctions is simply

$$\Phi_i = L_{ij} J_j \tag{4.3}$$

Fluxoid quantization requires that

Φ_i = (sum of the phases around the loop) - (-external applied flux)

By substituting this in equation 4.3, and inverting the matrix, the circulating currents are obtained. The total current through any junction is now the vector sum of the supercurrent and the circulating current. For non-zero current bias, the normal current through the junction is obtained from current conservation.

$$\text{Normal current} = I_b \pm J_j - I_c \sin(\phi_{ij}) \tag{4.4}$$

This is the current that contributes to the dissipation resulting in a finite voltage V. Therefore the voltage across the junction is proportional to the normal current and in normalized units,

$$V = I_b \pm J_j - I_c \sin(\phi_{ij}) \tag{4.5}$$

From Josephson's second relation, this is equal to the time rate of change of the phase.

$$d\phi_{ij} / dt = I_b \pm J_j - I_c \sin(\phi_{ij}) \tag{4.6}$$

for each junction. This is a first order differential equation in the phase drop. The equation is analytically solved for the phase using the Fourth order Runge Kutta technique.

The phases thus obtained satisfy fluxoid quantization, current conservation and the Josephson relations. The energy of the cluster is now obtained by summing up the individual junction energies. For low β, the contribution of the inductance to the energy can be ignored.

This gives the energy of the cluster in phase space for a random set of phases. To obtain the minimum energy, the phases are time stepped and the whole procedure is repeated till a minimum is found.

Contribution to the energy of the inductance: For high β, the inductive energy cannot be ignored. Each junction contributes a $\frac{1}{2} L I_s^2$ to the energy where L is a quarter of the loop inductance and I_s is the supercurrent through the junction. By summing up the contribution of each junction, both the self and the mutual inductance are taken into account.

Contribution to the energy due to finite current bias: For a non-zero current bias, the energy is given by

$$E_c = E_J \cos(\phi_{ij}) - \frac{E_J}{I_c} (I \phi_{ij}) \qquad (4.7)$$

where I is the total current through the junction.

4.21 Results of the simulation

The energy vs. flux have been obtained for arrays varying in size from 2x2 to 4x4. The smallest periodic unit of an array is a 2x2 and it is the smallest cluster that we choose to study. The 2x2 (with superconducting bus bars on two sides for current injection and removal) consists of six vertical junctions and two horizontal junctions. The energy of the cluster is simply the sum of the Josephson energies of each junction. For zero current bias and integer values of field, this energy is -8 E_J. For non-integer values of field, the system is frustrated. Fluxoid quantization requirements lead to generation of circulating currents which cause the system energy to increase. However, there are still some values of field at which the energy is a local minimum. Figure 4.2 is a plot of the energy vs. flux for a 2x2. There are five branches and the energy is symmetric about f=1/2 (as expected from the Hamiltonian). Each branch corresponds to a certain fixed number of vortices in the array. The first branch is the variation in energy with flux for the zero vortex case. The energy increases from f=0 because circulating currents are generated to cancel the applied field. At f=0.18, it becomes energetically favorable for the cluster to let one vortex in. The vortex can occupy one of four cells and the energies for these four positions is degenerate. At f=1/4 per cell, the energy is minimized because it corresponds to one vortex in the whole cluster and circulating currents are minimized. The middle branch is the two vortex state. Here two possible metastable states exist. The vortices can either exist next to each other or diagonally opposite from each other.

Fig: 4.2 Energy vs. flux simulation for a 2x2 cluster

The configuration with the vortices diagonally opposite each other has the lower energy (vortex-vortex) interaction is repulsive and the energy is minimized if the distance is maximized) and is the branch seen in the energy vs. flux curve. Note that there is a minimum at f=1/2. The three vortex branch is a mirror of the one vortex branch. Again four degenerate configurations exist. The four vortex state is also a mirror of the zero vortex state. Since there is a vortex in each cell, the circulating current in each cell is zero which is similar to the zero vortex case. The mirror symmetry about f=1/2 can be interpreted in terms of this by invoking the equivalence of a vortex to an antivortex. (An antivortex is the same as a vortex but with the field in the opposite direction i.e. the circulating currents in the cell flow in the reverse direction). The energy branches for f greater than 1/2 can be interpreted in terms of antivortices. Having three vortices in an array can be considered equivalent to having one antivortex. Figure 4.3 illustrates the equivalence in terms of the circulating currents. In Figure 4.4, the energy vs. flux has been plotted for six different cluster configurations. Note that the number of minima in the graph is size dependent. Each minimum corresponds to a field $f = p/(M*N)$ per cell. (where M x N is the cluster size consisting of M rows and N columns). For these values of f, there is an integer number of vortices (i.e. p vortices) in the cluster and these vortices arrange themselves so as to maximize their distance from each other. This results in a periodic arrangement of the vortices (a vortex lattice) which is commensurate with the underlying array lattice. This results in a reduction in the net circulating currents which are generated to satisfy fluxoid quantization. The energy is therefore a minimum for these values. The minimum at f=1/2 has the lowest energy as it corresponds to a vortex in every alternate cell.

In the presence of a small bias current (not large enough for the junctions to go into the free running state), the degeneracy of the vortex positions in the cluster is broken.

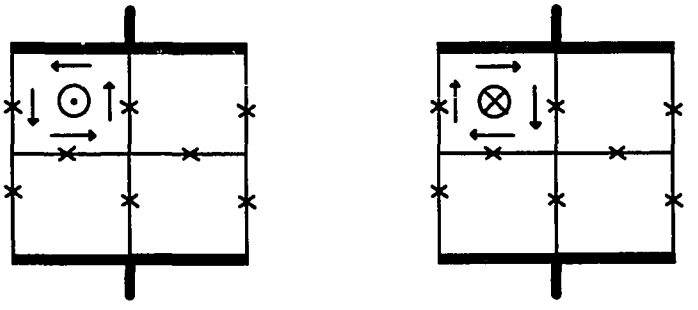

vortex anti-vortex

× – weak link ○ — direction of magnetic field

Fig: 4.3 Vortex and Antivortex in a Cluster

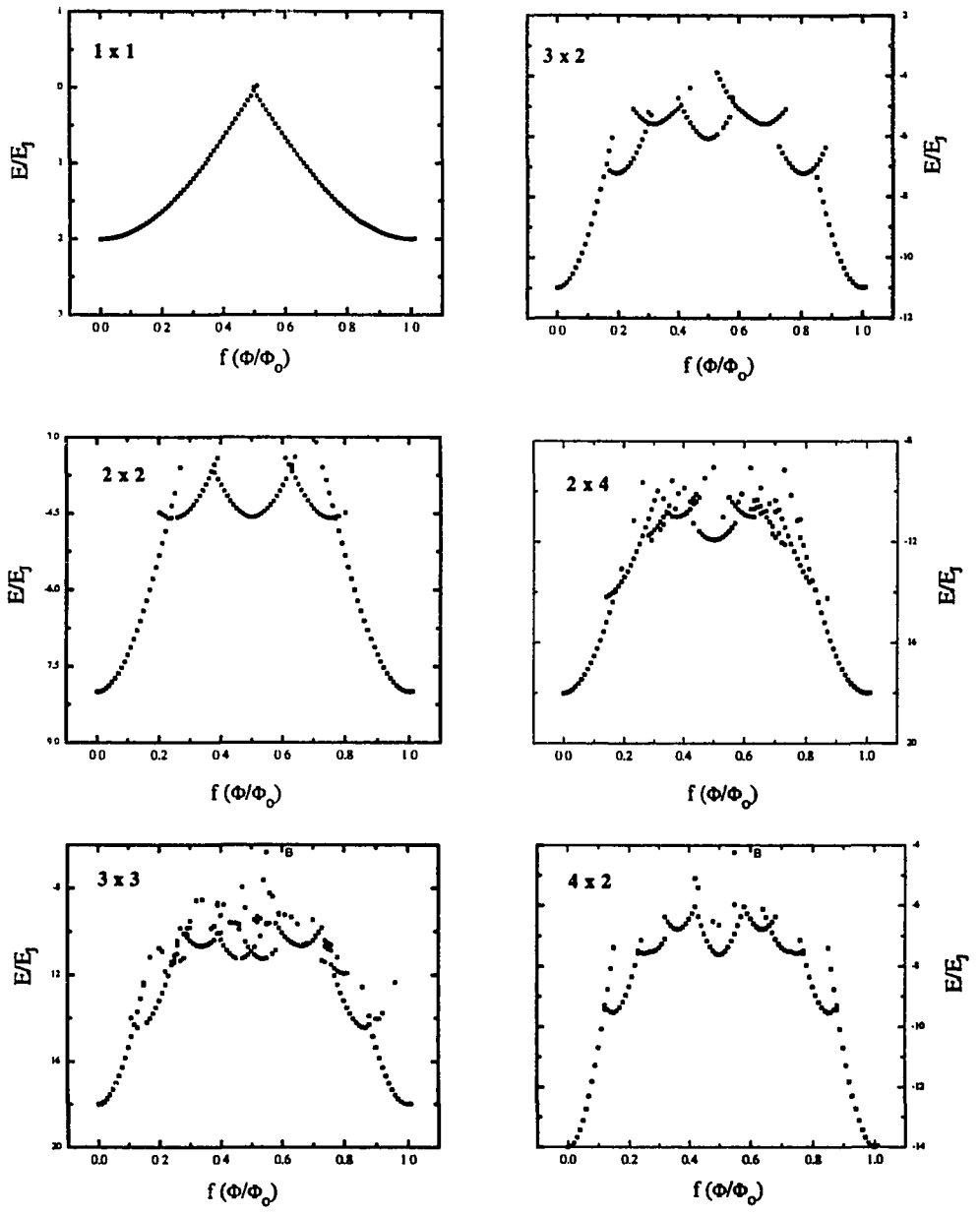

Fig: 4.4 Energy vs. flux for six cluster sizes

Depending on the direction and the magnitude of the current, some cells are preferred over others.

4.3 Dynamic properties:

From Josephson's second relation, evolution of junction phases gives rise to a finite instantaneous voltage. The measurements are made on a time scale much greater than that of the phase evolution and hence the quantity that is measured is the time-averaged voltage. Our simulations are designed to obtain this time averaged response.

The steps to calculate the voltage are similar to that for obtaining the energy. The input parameters are the same. The phases are initialized by choosing them randomly. The inductance matrix is calculated and inverted to get the circulating currents. In the energy vs. flux program, the Runge Kutta technique is used to obtain the phases as a function of time. The derivatives are also proportional to the voltage. This is the instantaneous voltage at each time step. The voltage is periodic in time with an oscillatory frequency equal to the Josephson frequency of the junction. The sum of the instantaneous voltages across each vertical junction, normalized by the number of columns, gives the voltage across length of the cluster. This is averaged over a finite set of time steps to obtain the average voltage. This time averaged voltage is equivalent to the quantity that is measured.

In Figure 4.5, the Voltage vs flux simulations for three different cluster sizes are shown. These are the results for a uniform cluster with a loop inductance $\beta=0.5$. Note that the number of minima scales with cluster size just like in the energy vs. flux case. The positions of the minima also mimic the energy vs. flux case. This similarity is not obvious. At rational values of f, the vortex lattice is commensurate with the underlying array lattice at equilibrium. In the presence of a bias current, a Lorentz force acts on

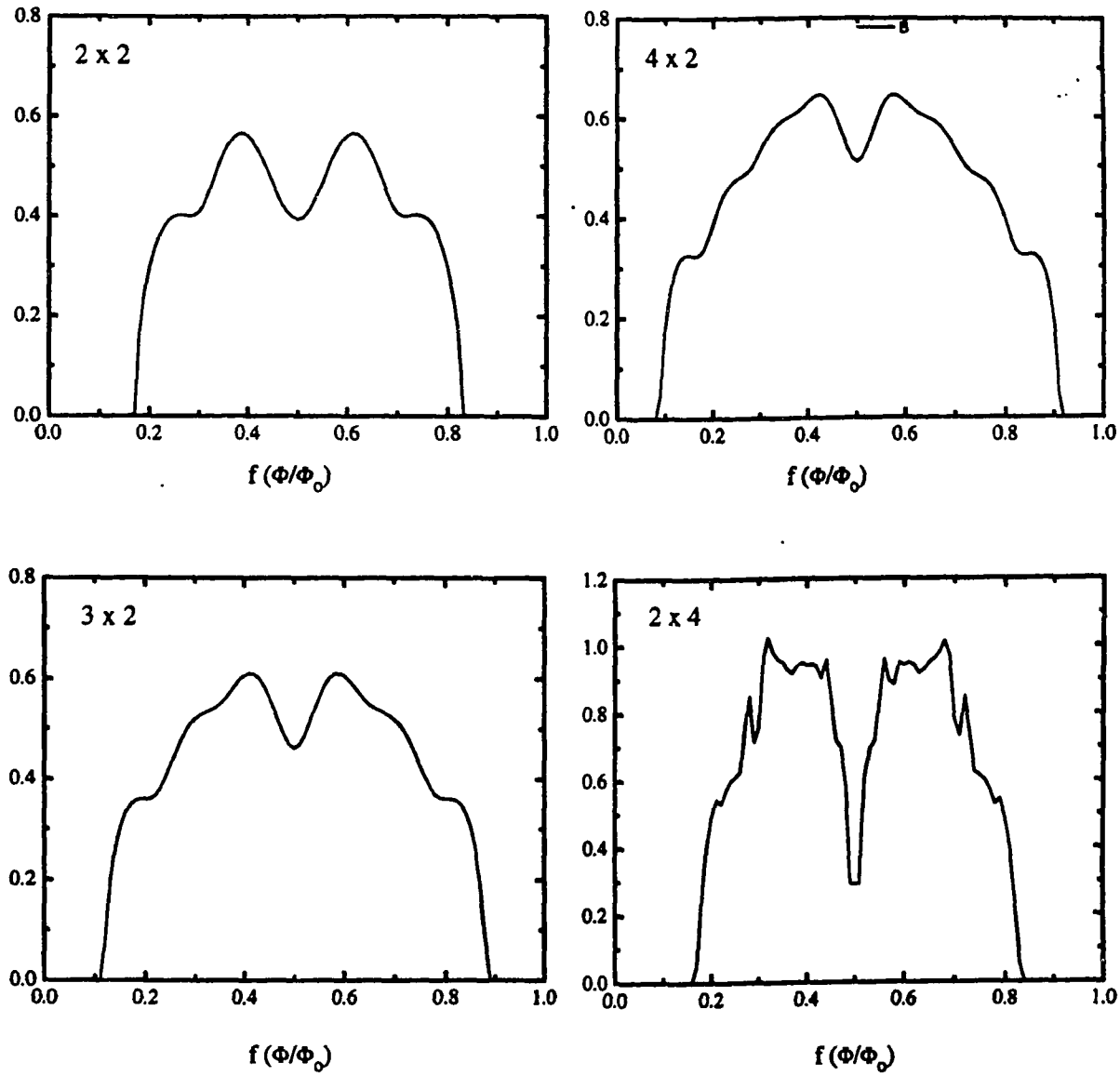

Figure 4.5 Voltage vs. flux simulations

these vortices. It is harder to distort the whole vortex lattice (by the Lorentz force) and this results in a lowering of the voltage at values of f where the energy is a minimum. The washboard potential model for a single junction involves the motion of the phase particle in a washboard-like potential in phase space. The motion of a vortex across the junctions of an array in real space can be described in a similar way. As discussed in Section 3.1, the array provides a uniform lattice of pinning sites for the vortex.

4.4 Sample preparation

The cluster samples are made using the same two step process discussed in Sec 3.2. We have made samples of Pb-Cu-Pb, Nb-Cu-Nb and Nb-Al-Nb. Each have their advantages and disadvantages. Each cluster mask has six clusters (2x2, 3x2, 4x2, 2x4, 3x3 and 4x4). Fig: 4.6 is a schematic of the cluster mask

The Experimental Setup

The experimental setup is also the same as discussed in Section 3.3. The voltage levels are much lower in this case (since there are less than five junctions in a column contributing to the voltage as opposed to hundreds of junctions in the case of a large array). The experiment is also more susceptible to noise.

Some of the measurements were made using the Internal Feedback technique. In this technique, the SQUID pickup coil and the sample are in parallel. Current injected into the current leads of the sample, divides itself between the sample and the pick up coil so as to satisfy current conservation and maintain the same voltage across both. The sample current changes if sample resistance changes (which happens if the magnetic field is changed) so as to keep the voltage across the SQUID and the sample equal. This technique is useful since it enhances the minima and maxima.

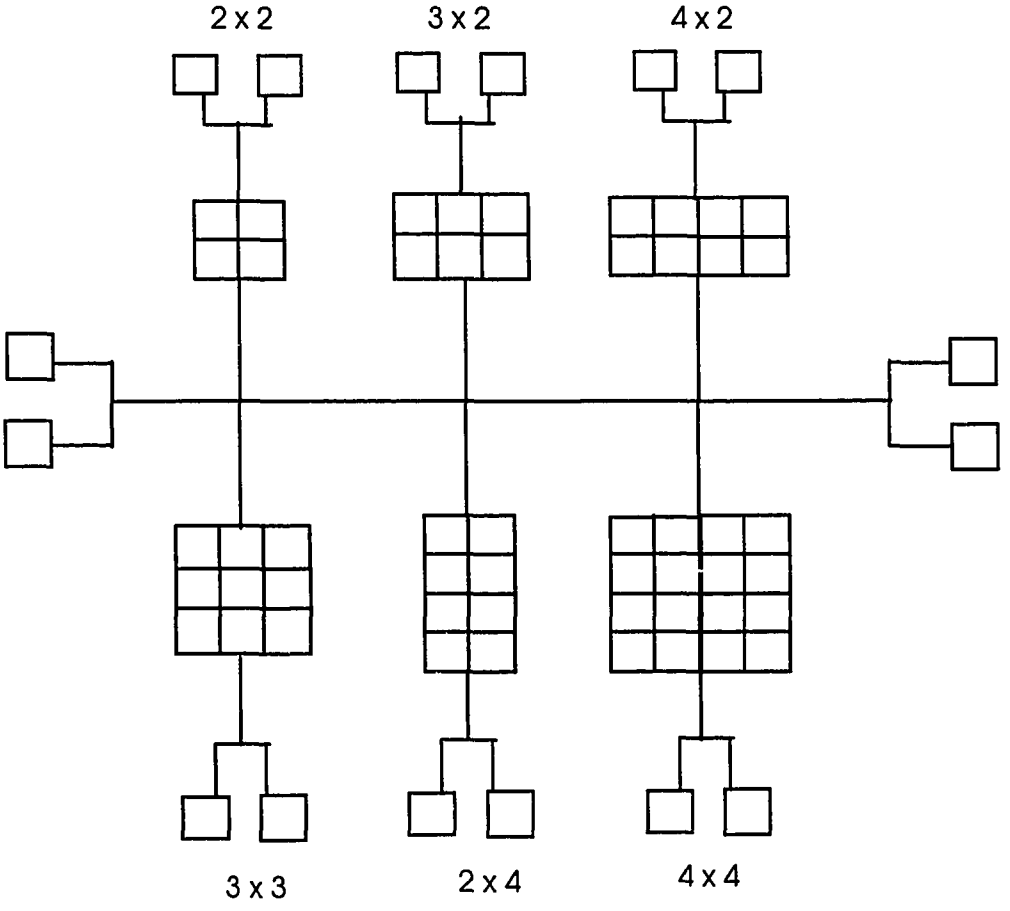

Fig:4.6 Cluster mask

4.5 Data:

Transport measurements have been made on 2x2, 3x2 and 4x2 and 3x3 sizes of clusters. The resistance as a function of applied field for constant I_b and T as well as the resistance as a function of temperature for constant I_b and f have been measured.

4.5.1 Voltage vs. flux data

The voltage was measured as a function of magnetic field for different cluster sizes. From the simulations we expect the number of minima to scale with the cluster size. Figure 4.7 is a plot of the data for a 3x2 (Pb-Cu-Pb) cluster measured at T = 1.95 K. The data shows the five features corresponding to commensurate fields at f = 1/6, 2/6, 3/6, 4/6 and 5/6. The peaks are not symmetric about f=1/2. As the bias current is increased from 0.5 μA to 2.9 μA, the depth of the minima decrease and the voltage increases. The positions of the minima however stay fixed. The reponse to bias current is due to an increase in the Lorentz force acting on the vortices which enables them to overcome the pinning potential of the cluster lattice.

Figure 4.8 is the voltage vs. flux reponse for a 4 x 2 cluster which has 2 rows, 4 columns and eight cells. The simulation indicates that there should be 7 commensurate vortex configurations at f = n/8 (n = 0,..8). The minimum at f = 7/8 is missing though its mirror minimum at 1-f (1/8) exists. The data is not symmetric about f=1/2. The features tend to wash out as the bias current is increased and at I_b of 3.98 μA, they are completely washed out. This is the depinning current for this cluster. The curve at I_b of 3.63 μA shows a retrace. The retrace shows a slight shift in the positions of the minima.

It is also of interest to compare clusters which have the same number of cells but have different geometries. This is shown in Figure 4.9 which shows the

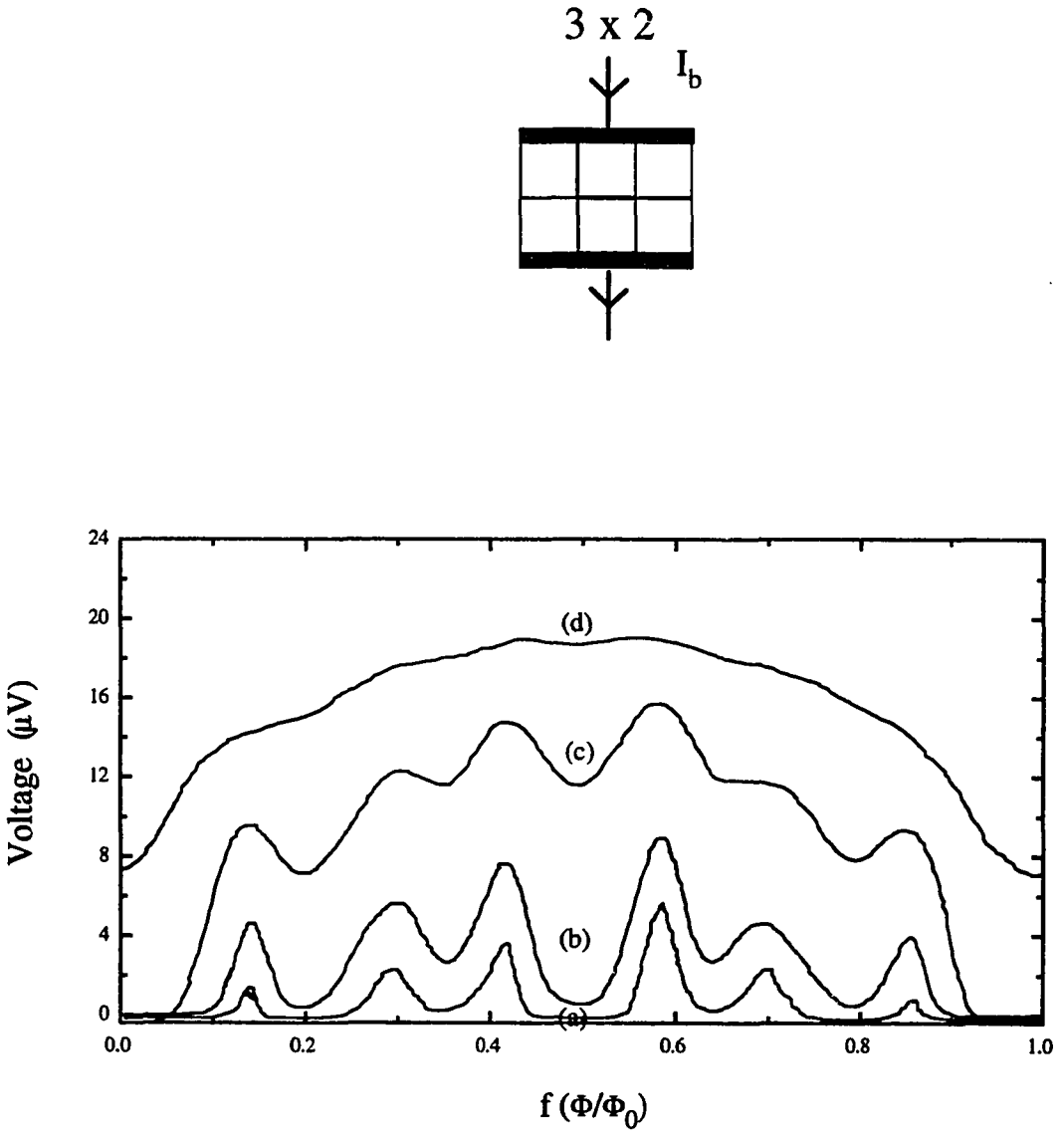

Fig: 4.7 Voltage vs Flux at T = 1.95 K
Bias currents of (a) 0.5 μA (b) 1 μA (c) 1.8 μA (d) 2.9 μA

4 x 2

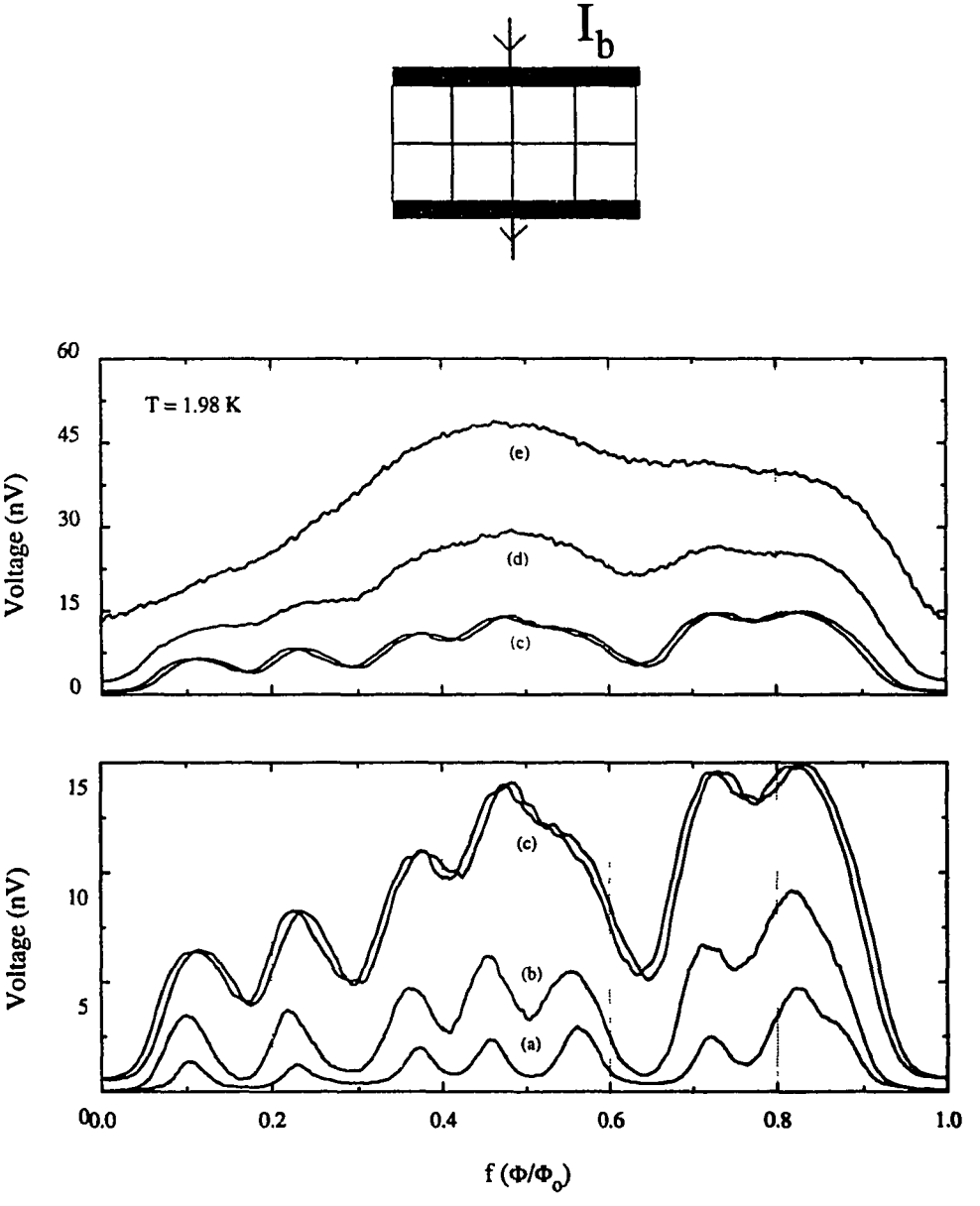

Figure 4.8 Voltage vs. flux for a 4x2 cluster
(a) 0.87 μA (b) 1.49 μA (c) 2 μA (d) 3.63 μA (e) 3.98 μA

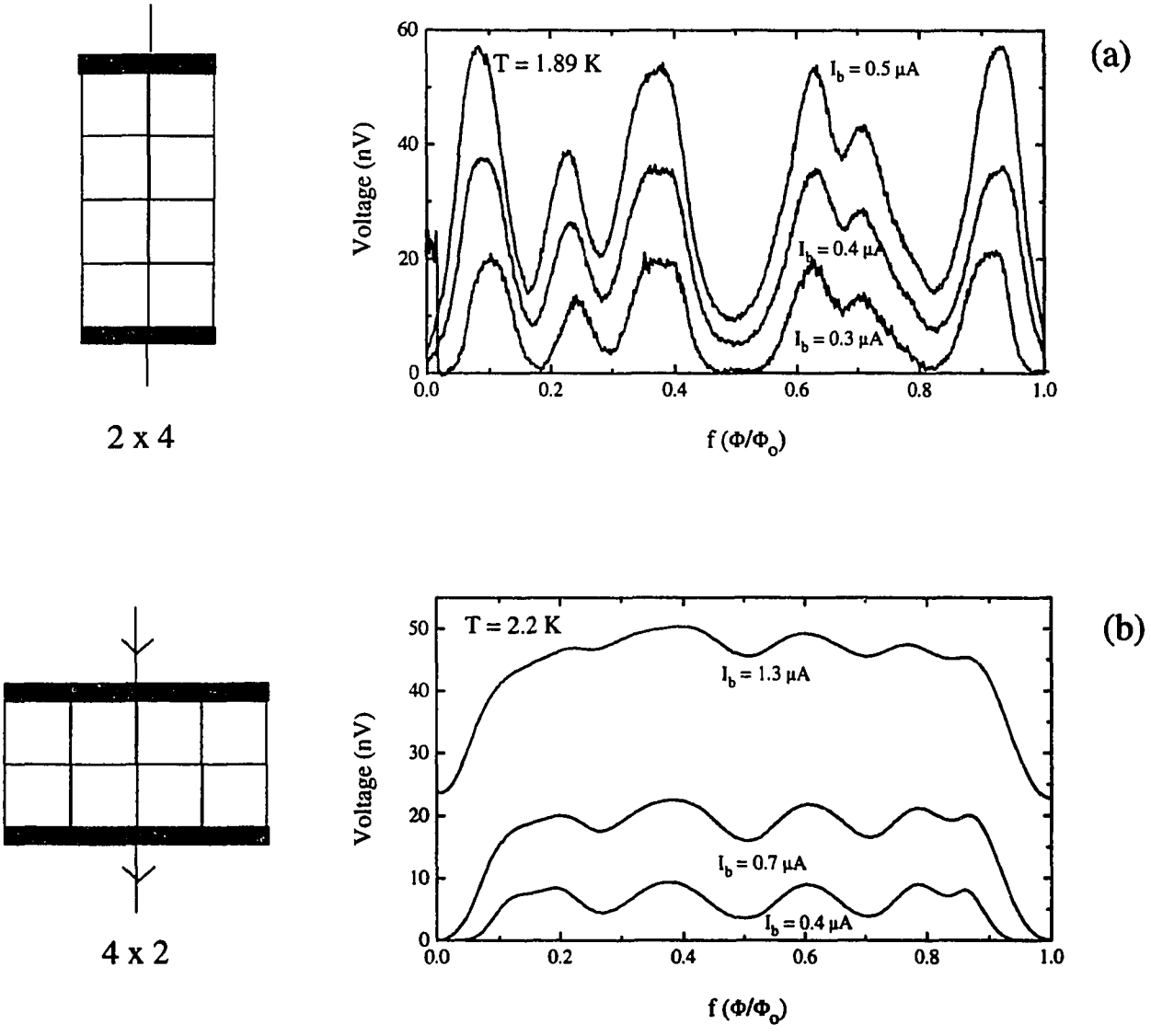

Fig: 4.9 Voltage vs. flux for two clusters (Pb-Cu-Pb) on the same substrate

magnetoresistance data for a (Pb-Cu-Pb) 2 x 4 and 4 x 2 cluster for different bias currents. Both the clusters show missing features and also exhibit asymmetry. The two systems do

not have the same dynamical behavior. The vortex motion in a 2 x 4 involves crossing three junctions whereas the motion in 4 x 2 involves crossing five junctions.

The data shown so far has been on asymmetric clusters. Figure 5 is the magnetoresistance data for a square 3 x 3 (Pb-Cu-Pb) cluster at T = 2.2 K (just below the transition temperature for the cluster) for different bias currents. The minima at 4/9 is mssing and the plot is asymmetric about f=1/2. Once again, the features are reproducible over a range of bias currents and their positions are the same.

To get a better understanding of the physics of these clusters, we conducted measurements on the simplest, non-trivial square cluster which is the 2x2.[9] The magnetoresistance data for a 2 x2 Pb-Cu-Pb sample (C6) is shown in Figure 5.1(a), for a range of bias currents at T=1.3 K. As the total bias current is lowered, the substructures at fractional values of f become more prominent. The three minima at f=1/4, 1/2, and 3/4th correspond to regions where the vortex lattice is commensurate with the underlying lattice. As discussed in section 4.1, these minima correspond to the minima in the energy.

In Figure 5.1(b) we show measurements of the voltage vs. flux for a 2x2 cluster (I_b = 17mA) for both polarities of magnetic field and bias current. Although the voltage is still periodic in the flux, the mirror symmetries about f=0, I=0, and f=1/2 are not present. Relative to the perfect array, some features are enhanced and others suppressed. This asymmetry could be due to trapped flux or inherent disorder in the cluster. If it is trapped flux, then we do not expect the asymmetries about f=1/2 and f=0. The trapped flux will only result in a shift of the voltage vs. flux. The disorder in the clusters could be

3 x 3

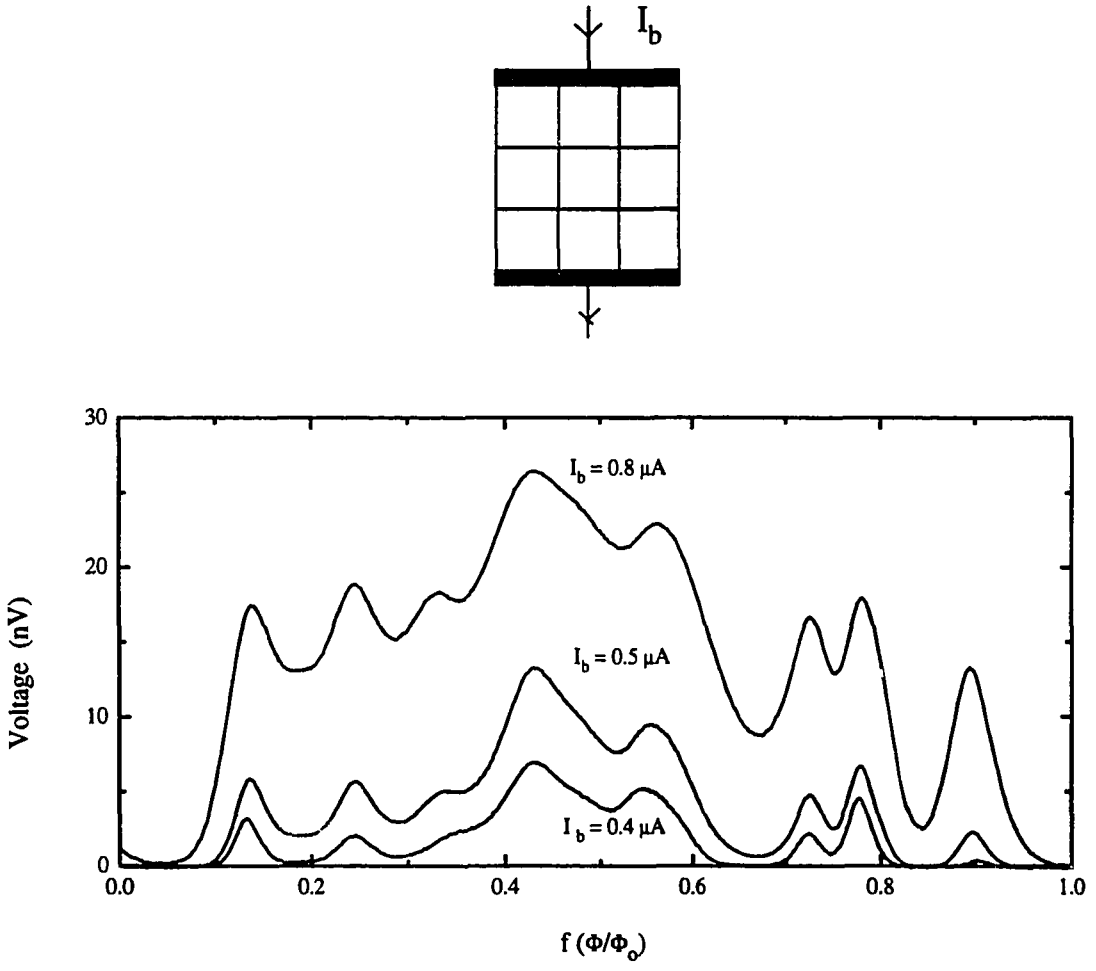

Fig: 5.0 Voltage vs. flux for a 3x3 cluster (Pb-Cu-Pb) at T = 2.2 K

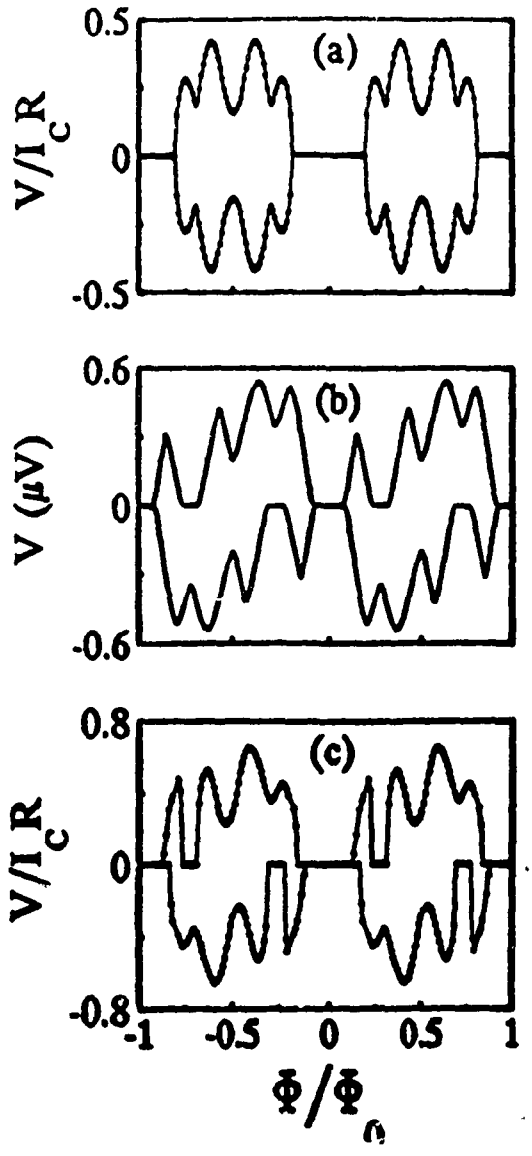

Figure 5.1 (a) Voltage vs. flux simulation for an ideal 2 x 2 cluster

(b) Voltage vs.flux data for a (Pb-Cu-Pb) cluster

(c) Voltage vs. flux simulations for a 2 x 2 cluster with critical current disorder

in the area or in the critical currents of the junctions. From SEM micrographs, it is apparent that the percentage variation in area is small enough to be discounted. Further, simulations with area disorder do not give the strong asymmetric features observed in the data. We carried out simulations with both random coupling disorder and specific junction disorder. Random disorder again caused only a smearing out of the voltage vs. flux. However, as shown in Figure 5.1 (c), we obtain reasonable agreement with the data by assuming that several of the junctions have substantially (up to a factor of two) different critical currents from the rest. Although the fit is not exact, the relative size and location of the principal features in the data are reproduced. Further, the dependence on the polarities of the field and the current are accurately predicted. Another computer simulation fit to data from a Nb-Al-Nb sample is shown in Figure 5.2 along with the configuration of critical currents used in the modeling. The required variation in the critical currents for the junctions (50-100%) is typical for clusters we have fabricated and modeled. The critical current of an SNS junction varies as $\exp(-d / \xi_n)$, where d is the width of the proximity gap and the normal metal coherence length

$\xi_n = (hv_F l / 6k_B T)^{1/2}$ depends on the mean free path l and the Fermi velocity v_F of the normal metal.[6] Scanning electron microscopy indicates a proximity gap of $1.3 \pm 0.2 \mu m$, within the expected resolution of optical lithography. For our junctions, assuming a mean free path l limited by boundary scattering, we estimate ξ_n to be about $0.4\ \mu m$ at the coupling temperature of 2 K. Thus, lithographic variations in the gap width Δd should modify the critical current by $\Delta d / \xi_n \approx 50\%$, in reasonable agreement with our measurements. The S-N interface is also relevant. The effective gap is affected by the quality of the interface. Since the critical current depends exponentially on the gap, small variation due to non-uniformity in the lithography become important. Since we use the same fabrication techniques for our larger arrays, we expect the variation in critical

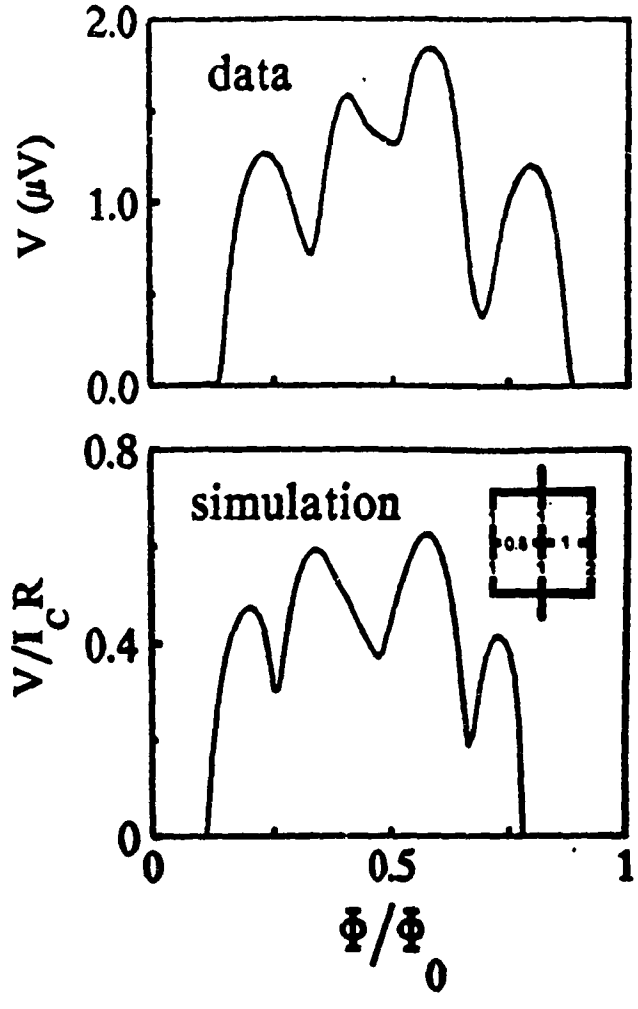

Figure 5.2 Voltage vs. flux for a 2 x 2 (Nb-Al-Nb) cluster

Simulation to match the data

currents to be comparable in those systems. However, due to averaging, the voltage-flux curves are always found to be nearly symmetric and lack sharp features. Although the disorder introduces asymmetry into the voltage-flux response, symmetry through the origin (f=0, I=0) and through the point (f=1/2, I=0). The inversion symmetries are apparent in both the data and the simulations. There is inversion through the origin is required by time reversal symmetry --- reversing both the field and current yields a distribution of total current (bias and circulating) time-reversed from the original current pattern. The inversion symmetry about f=1/2 is more subtle and depends on the dynamics of vortices and antivortices in the disordered cluster. This is discussed in the following section.

4.5.2 Analysis in terms of the spatial vortex motion across the 2x2 cluster

There are two possible techniques by which the vortex statics and dynamics in clusters can be modeled. One is in the phase space of the Josephson junctions and the other is in real space. Both models require knowledge of the potential energy distribution seen by a vortex. The potential energy distribution in phase space is a multi-dimensional washboard like potential whose dimensionality scales with the number of junctions. Vortices in this model can be interpreted as sums of phases around superconducting loops and their motion can be interpreted as due to phase slips across the junctions. This model gives a complete description of the system but it is complex and hard to visualize.

We use the real space model in two-dimensional space which is easy to visualize. It involves studying the pinning or motion of vortices in real space. The Josephson junction acts as a barrier to the vortex motion and the centers of the cells act as pinning sites. The potential energy distribution is similar to a single washboard potential in phase space. The model uses the basic principles of the phase space model to calculate the

barrier heights and the pinning energy. This makes it possible to calculate the stable vortex configurations of the system for different magnetic fields, and the response to bias currents. New vortex imaging techniques have made it possible to observe these stable vortex configurations for different magnetic fields and bias currents.

For zero bias current and temperatures below the transition, the vortices are pinned in the lattice of the cluster. The bias current applies a Lorentz force on the vortex and if it is large enough to overcome the pinning potential, the vortices move. This results in dissipation and hence a finite voltage as discussed in Chapter 3. The dynamic response of the system therefore depends on the equilibrium conditions. The asymmetry in the voltage response to field should be due to the asymmetry in the energy as a function of flux.

First, we examine the energy of the static vortex configurations vs. flux with and without bias current. This is shown in Figure 5.3(a) for the perfect 2x2 cluster. The energy scale is given in units of the Josephson coupling energy $E_J = I_c\Phi_0 / 2\pi$, where I_c is the average critical current of the junctions. A small bias current (small enough that the cluster is still in the superconducting state), results in a splitting of the energy levels for any given value of flux. The bias current breaks the degeneracy of the vortex positions in different cells. Note that the plot is symmetric about f=1/2. In Figure 5.3(b), the energy vs. flux for a 2x2 array is shown where one of the junctions has a different critical current from the rest. This coupling disorder also causes a splitting of the energy levels though the plot continues to be symmetric about f-=1/2. However, when a bias current is applied to the disordered cluster, the energy becomes asymmetric about f=1/2 due to the interaction of the bias current with the distorted circulating currents. We can explain these results by looking at the motion of vortices across the cluster which causes phase slips across the junctions. The vortex motion can therefore be mapped out in the

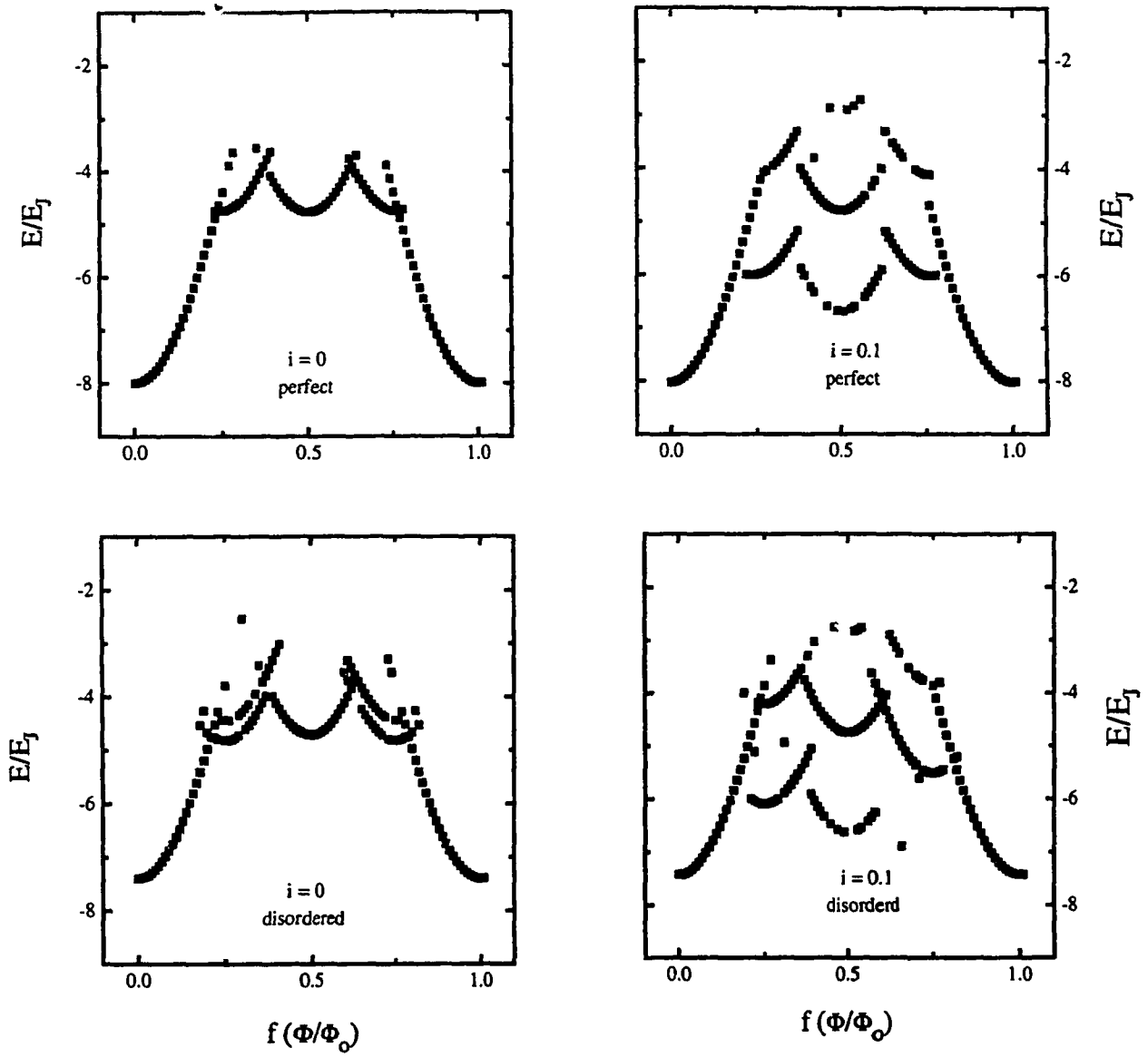

Fig: 5.3 Energy vs. flux for a 2x2 cluster for the ideal and the disorderd case and for zero and finite bias current

multi-dimensional phase space of the junctions. This is however quite complicated. The other option is to map out the motion in real space. The vortex moves in the potential offered by the Josephson junction lattice. To obtain this potential distribution, we need to know the barrier heights to vortex motion and the positions of minimum energy. For the case of the 2x2, there are four minimum positions. These are the centers of the four cells. As discussed in Chapter 3, a vortex in a Josephson junction array constitutes a sum of discrete phase drops across the junctions and circulating currents around the cell such that the fluxoid is quantized. When a vortex is at the center of a cell, all the junctions contribute to the phase drops and hence the circulating currents are minimized. When a vortex is "on" a junction, the phase drop across that junction is π and the energy of the system is a maximum. We calculate the barriers to vortex motion by holding the phase of the specific junctions to π. The minimum is obtained from the energy vs. flux program. It is important to point out that the energies thus obtained are only for specific positions along the cluster and not for each point in space. We have assumed a sinusoidal potential interpolation.

The results of the spatial potential distribution for the ideal cluster at zero bias and finite current bias is shown in the Figure 5.4 for f = 0.23. The middle barrier between the cells is about 1/5th of the entry barrier. The two minima have the same energy (degenerate). When a small bias current is applied, the potential tips over. As the bias current is increased, the entry barrier and then the other minima gradually disappear. The degeneracy of the two minima positions is broken. This is similar to the washboard potential in phase space where current causes the potential to tip over. In the case of the washboard potential, the current at which all the minima disappear is the critical current (also the onset of a finite voltage). The equivalent current for the spatial potential is the depinning current above which there is vortex motion which results in a finite voltage. For a bias current in the opposite direction, the potential distribution tips in the opposite

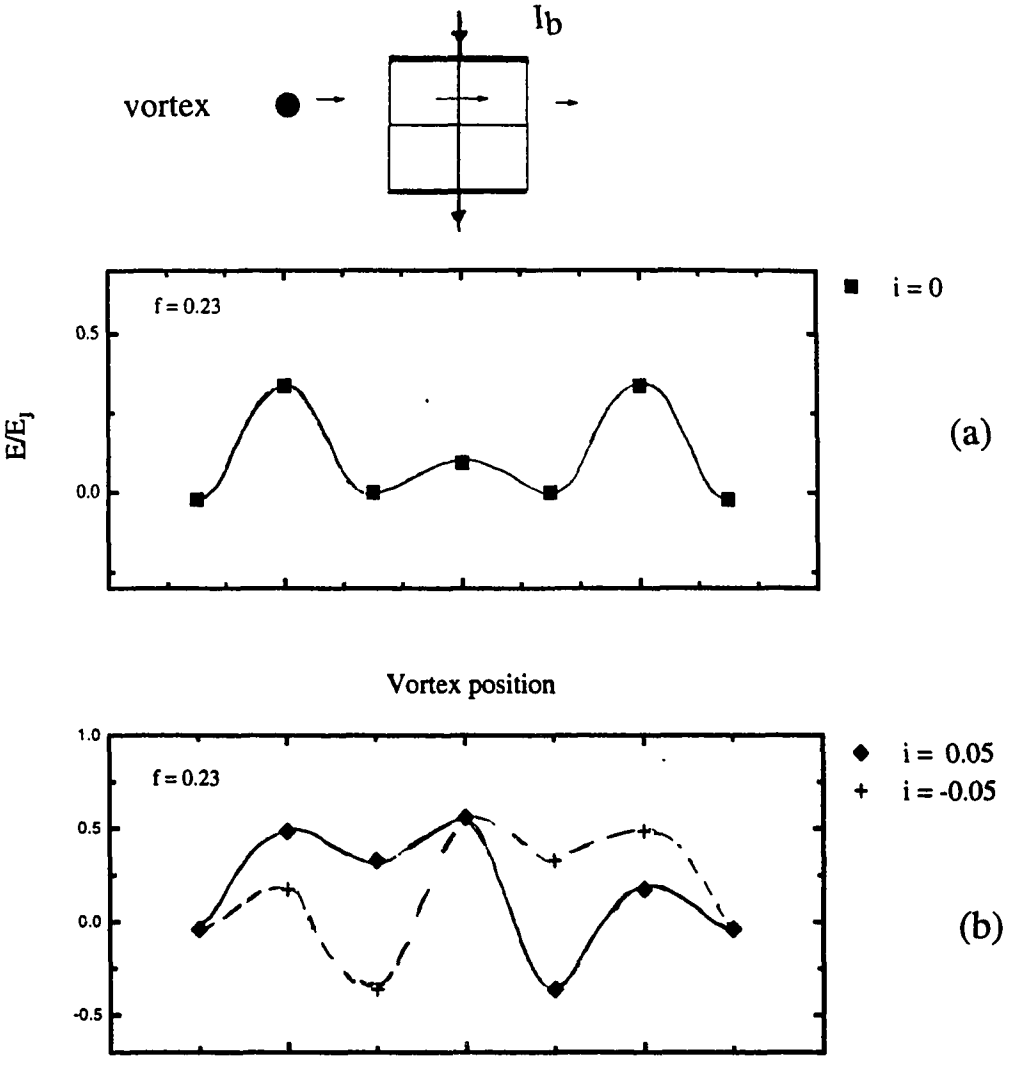

Figure 5.4 Spatial Vortex Potential for an ideal 2x2 cluster

(a) for opposite current polarities (b) for fields of f and (1-f)

direction. The magnitude of the slope and hence the voltage, is the same in both cases. To establish the equivalence between the state of the cluster at f and (1-f), we compare the potential distribution at f=0.23 with that at f=0.77 and this is shown in Figure 5.4 (b). The three vortex state has the minimum energy at this value of f. The distribution in space is obtained by looking at the collective motion of the three vortices. For zero bias, the distribution at f is the same as the distribution at (1-f). For a small bias current, however the tip at (1-f) is the opposite of that at f. Note that the

Figure 5.5 (a) and (b) shows the spatial potential distribution for the 2x2 cluster with coupling disorder for zero and finite current bias in both directions at f and (1-f). In this case, the tipping (and hence the slope) is different for the two directions of current. Also the slope at f for positive direction of current is equal to the slope at (1-f) for the negative direction of current. This explains the inversion symmetry about f=1/2 in the voltage vs. flux data for the 2x2. The same argument should hold for the 3x2 and 4x2 clusters. We have made the assumption that the vortex moves along a single row and does not cross between rows, which is not necessarily true.

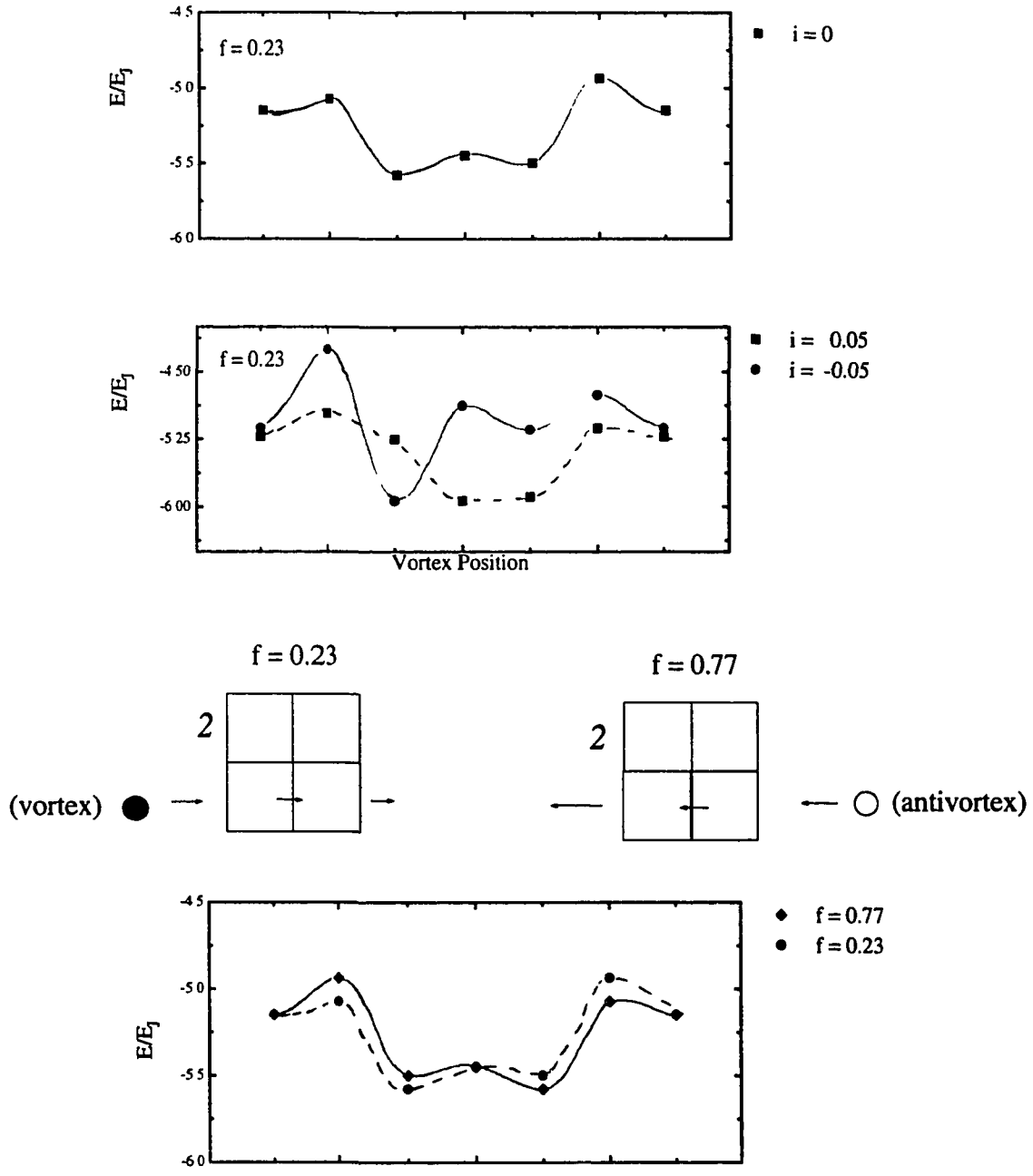

Figure 5.5 Spatial potential for a **disordered** cluster

4.5.4 Variation of spatial potential and barrier height with cluster size

The spatial potential for vortex motion has been calculated earlier for the 2x2. The spatial potential also scales with cluster size and this is depicted in Figure 5.6 (a) and (b). The barrier height due to the junctions is dependent on the junction position. The minima are deeper for those vortex configurations that are away from the edge of the cluster.

For a single junction, the net phase slip when a vortex crosses it is 2π. When the "vortex" is on the junction, the phase drop is π which corresponds to a maximum in the energy. This gives a barrier height for the junction which is equal to the E_J . As the size of the array increases, the barrier height drops to less than E_J. Such calculations have been done for large Josephson junction arrays by Rzchowskii et al. For the case of a 8 x 8 square array, they calculated the barrier height to be 0.2 E_J (the Josephson junction energy). The barrier heights for clusters lie in the intermediate region between that of large arrays and single junctions.

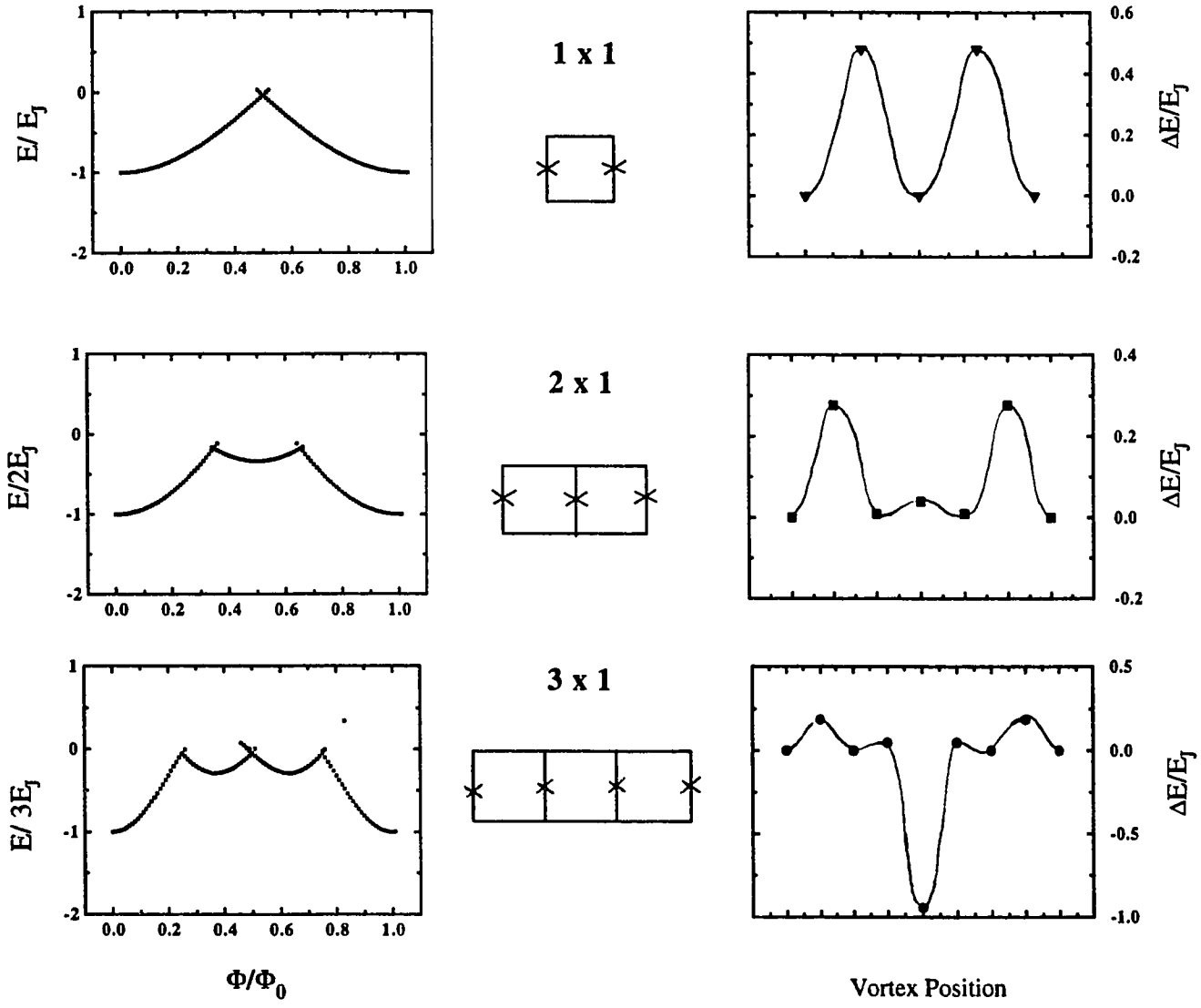

Fig: 5.6 Variation of the energy and potential with cluster size

4.6 Resistive transition

The data presented so far has been of the magnetoresistance of the clusters. It is also interesting to compare the resistive transition of large arrays with that of clusters. The resistive transition of large arrays has been described in some detail in Chapter 3. The arrays exhibit a thermal activation regime at low temperatures and a flux flow (Kosterlitz-Thouless) regime for higher temperatures. In Figure 5.7, the resistive transition of a 500 x 500 array and a 2 x 4 cluster have been plotted. The cluster transition should be similar to that for a single junction. The array has a smooth and broadened transition as opposed to the cluster which has a relatively sharp transition at a T = 1.5 K. The plot of log (R) as a function of (1/T) is linear for the large array. This indicates that over the temperature range, the transition is due to thermal activation of vortices (as discussed in Chapter 2). The same plot for the 2x4 cluster is non-linear indicating that the resistive transition mechanism is different. More work needs to be done for different magnetic fields and wider temperature ranges.

500 x 500

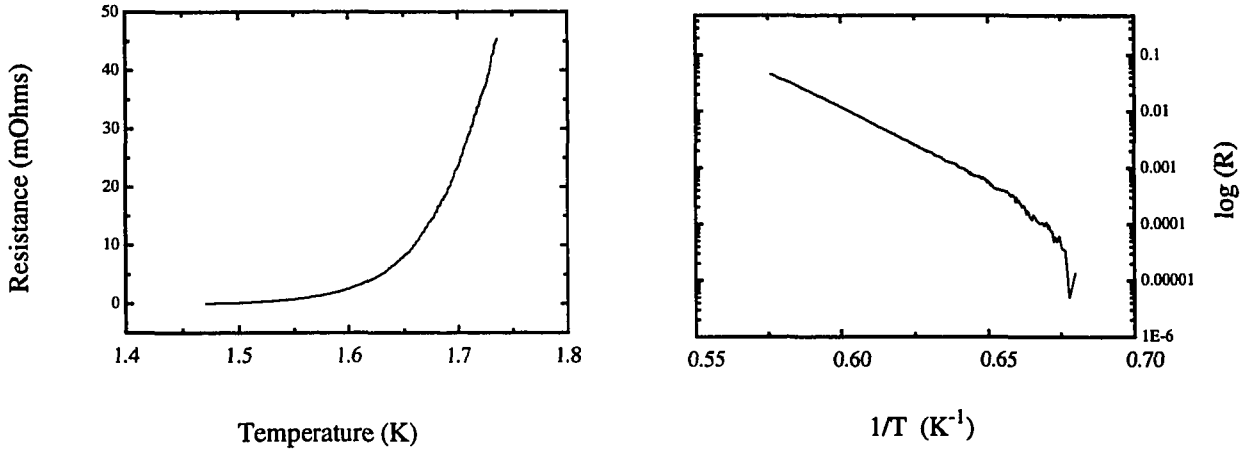

2 x 4

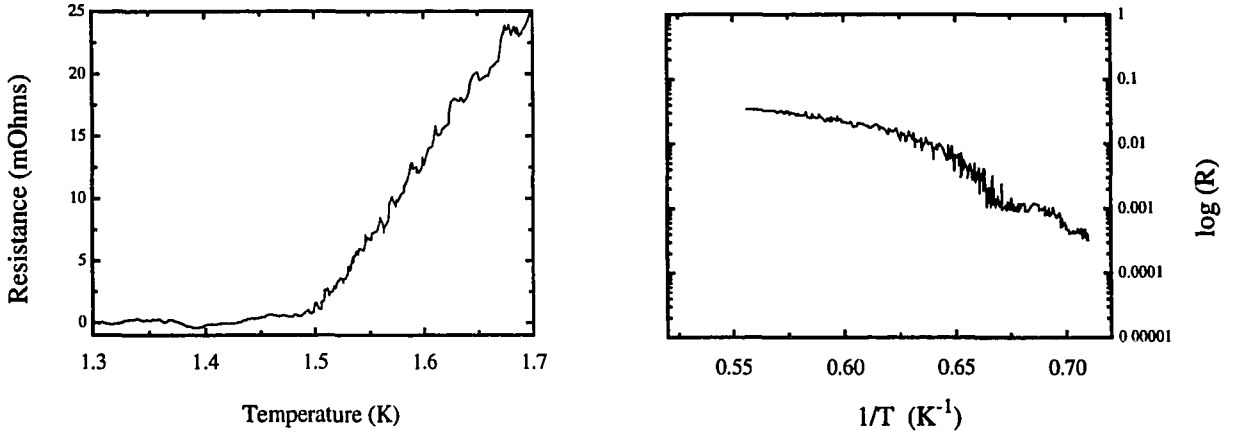

Fig: 5.7 Comparison of the resistance onset of a 2x4 cluster and a large array

REFERENCES

1. C. D. Tesche and J. Clarke, J. Low Temp. Phys. **29**, 301 (1977).

2. W.-T. Tsang and T. Van Duzer, J. Appl. Phys. **46**, 4573 (1975).

3. J. A. Blackburn, J. Appl. Phys, **56**, 1477 (1984).

4. P. Hadley and M. R. Beasley, Appl. Phys. Lett. **50**, 621 (1987).

5. J. H. Miller, Jr., et al, Appl. Phys. Lett., **59**, 3331 (1991)

6. P. G. de Gennes, Superconductivity of Metals and Alloys, Addison-Wesley Publishing Company Inc., California (1989)

7. M. B. Cohn, M. S. Rzchowski, S. P. Benz, and C. J. Lobb, Phys. Rev. B **43**, 12823 (1991)

8. F. Parodi and R. Vaccarone, Physica C **173**, 56 (1991)

9. Jinhee Kim and Hu Jong Lee, Phys. Rev. B **47**, 582 (1993);

   M. S. Rzchowski, L. L. Sohn, and M. Tinkham, Phys. Rev. B **43**, (1991)

   P. Hadley and M. R. Beasley, Phys. Rev. B **38**, 8712 (1988)

   W. Xia and P. L. Leath, Phys. Rev. Lett., **63**, 1428 (1989)

10. S. V. Rao and D. J. Van Harlingen, Phys. Rev. B **48**, 12853 (1993)

CHAPTER 5

FUTURE DIRECTIONS

In conclusion, we have studied both large Josephson junction arrays and clusters to obtain a better understanding of the statics and dynamics of vortices and their interaction with the underlying lattice. The effects of intrinsic inhomogeneity in the junction critical currents has been of particular interest. We developed a simple, single vortex picture to explain the vortex behavior in clusters.

The next obvious step in this regard is to fabricate clusters with known amounts of disorder and compare the voltage vs. flux response measurements with simulations of the same. We have already done some preliminary measurements on disordered clusters.

This is only the beginning of the work on clusters. It is a new regime of interest in Josephson junction arrays. Recent advances in vortex scanning techniques have made it possible to look at the static vortex configurations of an ensemble of clusters. Work in this direction is in progress in our own research group using the Scanning SQUID Microscope.[1] Calculations of stable vortex configurations for different magnetic fields and the knowledge of the barrier heights will be of particular relevance.

Various research groups have used small and large arrays to model HTSC systems. Experiments have shown that these films consist of grains of superconductor separated by weak links.[2] These weak links have a low critical current and hence degrade the critical current of the entire film. Therefore it is of interest to study these systems and a suitable model is a Josephson junction array.[3,4,5,6,7] These models have used small arrays like SQUID arrays, linear chains of jucntions, and networks to predict the properties of the film.

Another area where cluster like devices are of use is to make commercially viable devices like shift registers[8] in Josephson computers and the SQUIG (Superconducting Quantum Interference Grating) for detection of magnetic flux.

REFERENCES

1) For further information on this subject refer to Dr. Lan Vu's thesis

2) P. Chaudhari, J. Mannhart, D. Dimos, C.C. Tsuei, J. Chi, M. M. Oprysko and M. Scheurmann, Phys. Rev. Lett. **60**, 1653 (1988)

3) F. Parodi and R. Vaccarone, Physica C **173**, 56 (1991)

4) T. Yamashita and L. Rinderer, J. Low Temp. Phys. **21,** 153 (1975)

5) A. Giannelli and C. Giovannella, Proc. 3rd National Meeting on High Temperature Superconductivity, 358 (1990)

6) C. J. Lobb, D. W. Abraham and M. Tinkham, Phys. Rev. B **27**, 150 (1983)

7) Jerzy Zagrodzinski, Physica C **180**, 216 (1991)

8) T. A. Fulton, R. C. Dynes and P. W. Anderson, Proc. IEEE **61**, 28 (1973)

VITA

Subashri V. Rao was born on 24th September, 1966 in Madras, India. She completed her Bachelors degree in Engineering Physics from the Indian Institute of Technology, Bombay in 1987 and was the valedictorian of her class. She then proceeded to the United States to complete a Ph. D in Physics from the University of Illinois, Urbana-Champaign in 1994.